A Fluorescence-Based Coupled Enzyme Cascade Assay in the Investigation of Old Yellow Enzymes for Biopolymer Production

Jacob Sicheri

A Thesis
In
Department
Of
Biology

Presented in Partial Fulfillment of the Requirements
for the Degree of Master of Science (Biology) at
Concordia University
Montréal, Quebec

August 2023

CONCORDIA UNIVERSITY
School of Graduate Studies

This is to certify that the thesis prepared

By: Jacob Sicheri

Entitled: A fluorescence-based coupled enzyme cascade assay in the investigation of Old Yellow
            Enzymes for biopolymer production

and submitted in partial fulfillment of the requirements for the degree of

Master of Science (Biology)

complies with the regulations of the University and meets the accepted standards with respect to
originality and quality.

Signed by the final Examining Committee:

_____ Chair
Dr. Isabelle Benoit-Gelber

_____External
Dr. Steve Shih

_____Examiner
Dr. Isabelle Benoit-Gelber

_____Examiner
Dr. Paul Joyce

_____Supervisor
Dr. David Kwan

Approved by   _____

Dr. Robert Weladji, Graduate Program Director

August 28, 2023   _____

Dr. Pascale Sicotte, Dean of Faculty of Arts & Science

ABSTRACT

A Fluorescence-Based Coupled Enzyme Cascade Assay in the Investigation of Old Yellow Enzymes for Biopolymer Production

Jacob Sicheri

Plastics are a useful and necessary material in the modern world. However, the methods of extraction and the finite nature of petroleum necessitates divesting from traditional petroleum-derived plastics. One avenue being pursued is sustainably sourced plastics; namely plastics made from a biorenewable starting source. Enzyme catalysis and Old Yellow Enzymes (OYEs) in particular are of note in pursuing the generation of plastics from biorenewable sources. Engineering OYEs in pursuit of expanded substrate scope, improved efficiency, and other traits is growing increasingly popular and tools towards this aim remain valuable. In this work, I characterized, optimized, and utilized a novel fluorescence-based enzyme cascade in the investigation of nine candidate OYEs and their activities on four biorenewable plastic precursors. This enzyme cascade couples the redox activity of OYEs to the release of 4-methylumbelliferone, a fluorophore with a fluorescence intensity maximum at 445 nm. First the cascade was verified using Malate Dehydrogenase. This was followed by the optimization of the enzymatic cascade through the mutation of supporting enzyme GapA to utilize NADPH instead of its native NADH and the adjustment of NADPH concentrations to limit off-target fluorescence. Once optimized, the assay was utilized in a screen of nine OYEs with four biorenewable plastic precursors. Hits from the screen were investigated and the assay itself was investigated in the pursuit of enzymatic characterization. With a successful use-case demonstrated for this robust fluorescence-based activity assay, I was successfully able to add a tool to the development of OYEs towards generating sustainable plastics.

ACKNOWLEDGEMENTS

Contributions

I would like to thank everyone involved in the development of this project.

1. The design of the fluorescence-based activity assay utilized throughout Chapter 3 was developed by Dr. David Kwan. In these chapters, Jacob Sicheri conducted the experimentation and analysis of the data.

2. In Chapter 3, the LC-MS was done by Dr. David Kwan. Jacob Sicheri performed the reactions and conducted the analysis of the data.

All authors reviewed the final manuscript and approved of the contents.

Table of Contents

List of Figures

List of Tables

List of Abbreviations

(-)-β-methyl-δ-valerolactone ((-)MVL)

4-aminocinnamic acid (4-ACA)

4-aminohydrocinnamic acid (4-AHCA)

4-methylumbelliferone (4-MU)

4-methylumbelliferyl b-D-glucopyranoside (4MU-Glc)

6-phosphoglucoside-specific β-glycosidase (BglA-2)

8-hydroxypyrene-1,3,6-trisulfonic acid (HPTS)

12-oxophytodienoate reductase 1 (OPR1)

Adenosine Diphosphate (ADP)

Adenosine Triphosphate (ATP)

Alcohol Dehydrogenase (ADH)

Anhydromevalonolactone (AMVL)

Bacillus subtilis NADPH dehydrogenase (YqjM)

β-glucoside kinase (BglK)

Caprolactone and Globalide copolymer (PGlCL)

Column Volume (CV)

Deoxyribonucleic Acid (DNA)

Deinococcus radiodurans ene-reductase (DrER)

Electron Withdrawing Group (EWG)

Enoate Reductase *Clostridium acetobutylicum* (ER-CA)

Ferulic Acid Decarboxylase 1 (FDC1)

Flavin Adenine Dinucleotide (FAD)

Flavin Mononucleotide (FMN)

Gas Chromatography (GC)

Genomic DNA (gDNA)

Glyceraldehyde-3-phosphate (G3P)

Glyceraldehyde-3-phosphate dehydrogenase A (GapA)

Guanidine Diphosphate (GDP)

High Performance Liquid Chromatography (HPLC)

in vitro transcription and translation (IVTT)

Isopropyl β- d-1-thiogalactopyranoside (IPTG)

Lactic Acid (LA)

Liquid Chromatography Mass Spectrometry (LC-MS)

Malate Dehydrogenase (MDH)

Mass Spectrometry (MS)

Morphinone reductase (MR)

N-ethylmaleimide reductase (nemA)

Nicotinamide adenine dinucleotide (NADH)

Nicotinamide adenine dinucleotide phosphate (NADPH)

Old Yellow Enzymes (OYEs)

Old Yellow Enzyme 1 (OYE1)

Old Yellow Enzyme 2 (OYE2)

Old Yellow Enzyme 3 (OYE3)

para-methoxy-2-amino benzamidoxime (PMA)

Pentaerythritol Tetranitrate Reductase (PETNR)

Phenylalanine Ammonia-Lyase (PAL)

Phosphate-Buffered Saline (PBS)

Phosphoglycerate Kinase (PgK)

Polyethylene terephthalate (PET)

Polyhydroxyalkanoates (PHAs)

Polyhydroxybutyrates (PHBs)

Poly(lactic acid) (PLA)

Polymerase Chain Reaction (PCR)

Poly[(R)-2-hydroxybutyrate] (P(2HB))

poly(vinyl chloride) (PVC)

(R)-2-hydroxyglutarate dehydrogenase (Hgdh)

Ralstonia eutropha type I polyhydroxyalkanoate synthase (PhaC$_{Re}$)

Ralstonia metallidurans ene-reductase (RmER)

Relative Fluorescence Units (RFU)

Seamless Ligation Cloning Extract (SLiCE)

Terrific Broth (TB)

Thermoanaerobacter brockii Alcohol Dehydrogenase (TbSADH)

Uridine diphosphate (UDP)

Xenobiotic Reductase B (XenB)

Chapter 1 - Introduction

Traditional chemical synthesis of plastics and fabrics hinges on unsustainable practices stemming from the use of petrochemical materials to derive the vast majority of plastics we use today. Plastic use is ubiquitous within the modern world. As of 2019, plastic production reached the scale of 368 million metric tons [1] and that amount is predicted to double within the next two decades [2]. Most plastics used are synthetically-derived and their feedstocks consist of the direct resources or by-products of oil, natural gas, and coal extraction [3]. The extraction of petroleum has been significantly documented as being directly linked to human-driven environmental damage [4]. En-masse petroleum extraction has driven losses in biodiversity [5], has impacted human health in areas surrounding extraction sites [6], and is contributing to an increase in human activity-driven earthquakes [7]. The way plastics are made cannot coexist with sustainability goals set by many governments and the United Nations [8]. With petroleum extraction being a necessity for the production of the vast majority of plastics, the impacts to human health, animal welfare, and the environment beyond are intrinsically linked to the utilization of plastics. Beyond the impacts of extraction on health and the environment, petroleum remains a finite resource. While plastics will remain useful, petroleum reserves will eventually diminish, highlighting a need to divest from petroleum-derived plastics. With these issues in mind, two schools of thought exist. One: divest away from single-use plastic use to more reusable packaging, fabrics, and consumables. Or two: replace the utilization of fossil fuels with a more sustainable alternative for plastic generation. In reality, both ideas will likely be necessary to achieve a more sustainable future for plastics. This is because not everything made from plastics currently can be replaced with a more reusable alternative. For example, since their inception in the 1960s, plastics have become ubiquitous in the medical field, particularly with medical devices. For the medical field to divest from single-use, sterilized plastic devices would require an immense shift in medicine that is unlikely to happen overnight [9]. Nonetheless, a clear need exists to diverge from traditional chemical synthesis derived from petrochemicals, in plastics and beyond.

1.1 Green Chemistry and Biocatalysis

With the ongoing paradigm shift towards a cleaner, more sustainable future, enzyme catalysis and green chemistry provide a potential opportunity to usher in sustainable alternatives.

Green chemistry and the role enzymes play in that field has been well established since the 1990s when the term "green chemistry" was coined [10]. Green chemistry as an idea was initially proposed by Paul Anastas and John Warner in 1998 [11] and the idea revolves around the minimization of the environmental impact of chemistry. Anastas and Warner outlined twelve principles of green chemistry to these ends which have guided the development of the field. In 2003, Gonzalez and Smith added an additional twelve principles which further enhanced the originals. With these 24 guiding principles in mind, green chemistry has evolved to be at the foundation of much of the ongoing discovery of environmentally benign chemistry. As noted by Leitner et al [12], many developments within the field have been made towards nondepleting, nontoxic, and nonpersistent chemicals. For nondepleting, much work has been done towards utilizing renewable feedstocks like lignocellulose [13] or reusing existing waste [14] [15] as starting materials for chemical reactions. For nontoxic chemistry, ongoing efforts focus on finding alternatives to existing toxic solvents [16] and catalysts [17]. Finally, nonpersistence focuses on the ability of chemicals to remain only for a short period of time in the environment before breaking down to non-toxic degradation products. Plastics in particular are a focus for this segment of green chemistry as plastics are increasingly found in organisms from crabs to seabirds to fish [18] [19] as microplastics. Microplastics are also increasingly found in humans and may have significant impacts on human health [20]. To this end, green chemistry seeks to identify plastics that are biodegradable and have low environmental impact. In 2017, Zhu *et al.* [21] investigated the addition of isosorbide diester to poly(vinyl chloride) (PVC) blends to replace petrochemical-derived phthalates. Isosorbide diesters are readily biodegradable and non-toxic, rendering this PVC blend much more in line with green chemistry principles. In another example, Guindani *et al*. [22] investigated a caprolactone and globalide copolymer (poly globalide-co-epsilon-caprolactone poly(epsilon-caprolactone)) (PGlCL) with additional post-polymerization *N*-acetylcysteine modification for hydrolytic, enzymatic, and microbial action. They found that this modified PGlCL was much more readily degraded in all conditions including biodegradation by microbial solution. While unmodified PGlCL is already used as a biodegradable polyester in biomedical [23] applications, the existing long degradation time was a downside that seems to have been improved by the modification that Guindani and team have introduced.

Progress in green chemistry has not been solely limited to improving traditional chemistry. Biochemistry has increasingly been investigated as an avenue for green chemistry development.

Enzymes are recognized as being a source of opportunity for green chemistry due to the nature of enzymatic reactions occurring in mild conditions with little need for extreme pressure, heat, or addition of toxic catalysts or cofactors. In fact, biocatalysis readily satisfies 11 of 12 of the green chemistry principles established at the advent of the field [24] (Table 1).

Table 1: Satisfaction of green chemistry principles by enzyme catalysis (Adapted from Cipolatti et al [24]).

Green Chemistry Principles	Enzymatic Biocatalysis Principles
Waste Prevention Instead of Remediation	Minimization of by-products avoids waste generation
Atom Economy	High selectivity and efficiency
Use of less hazardous and toxic chemicals	Enzymes perform catalysis in mild conditions
Safer products by design	Enzyme catalysis mostly generates non-toxic products
Innocuous solvents and auxiliaries	Enzymes perform catalysis in mild conditions
Energy efficiency by design	Enzyme catalysis takes little energy for catalysis (mild temperatures and pressure)
Preferred use of renewable raw materials	Enzymes are renewable through recombinant expression
Shorter syntheses (reduce derivatives)	High activity, specificity, and conversion yields
Catalytic rather than stoichiometric reagents	Enzymes are catalysts by nature
Design products to undergo degradation in the environment	Enzymes are biodegradable
Analytical methodologies for pollution prevention	Beyond the scope of enzyme catalysis alone
Inherently safer processes	Enzymes perform catalysis in mild conditions

Biocatalysis has grown to fill a wide range of niches and support existing reactions within green chemistry from biofuel generation [25] of pharmaceuticals [26]. Of particular interest to this

project are enzymatically-derived plastics and fabrics.

1.2 Bioplastics and Enzyme Catalysis

Much research has been devoted to the investigation of enzymes for plastic degradation, particularly in the area of polyethylene terephthalate (PET) breakdown through a wide variety of enzymes catalyzing PET hydrolysis [27] [28] [29]. However, enzymes can provide value to the generation of plastics as well through direct enzymatic catalysis and whole organism biotransformations. As stated above, current petrochemical derived plastics pose a significant issue in their starting feedstocks. To supplant these feedstocks, many groups are investigating instead the use of renewable feedstocks to generate plastics. Bioplastics are a subset of plastics that are made from renewable feedstocks and are often (but not required to be) biodegradable. In 2020, the bioplastic market reached $10 billion USD and is continuing to expand [30]. Current bioplastics are made from a wide variety of sources. Poly(lactic acid) (PLA) polymers are among the most popular bioplastics with the largest consumption volume of any bioplastic [31]. The vast majority of lactic acid (LA) used for polymerization is from a renewable feedstock via microbial fermentation by a *Lactobacillus* species [32]. While in previous years simple carbohydrates were used as a feedstock for this fermentation, progress is ongoing to use more sustainable carbohydrates such as waste whey [33] and lignocellulose [34] [35]. While PLAs are the most abundant bioplastic, they also suffer from drawbacks that make them inferior to petrochemical derived plastics. One of the major downsides of PLA (common to all bioplastic) is cost. Current manufacturing of PLA still does not compete with conventional plastics production [36]. Costs for the manufacturing of PLA are estimated by [36] at $US 2.71/kg PLA which is almost double the average price of comparable thermoplastic polystyrene ($US 1.6/kg) [37]. However ongoing efforts to utilize waste inputs along with ongoing titer increases [38] and strain optimization [39] is predicted to reduce costs lower and lower. The role of enzymatic catalysis should not be understated in the production of PLAs and efforts have been ongoing to investigate new enzymes [40] or improve existing enzymes [41] for the production of PLAs.

Not limited to PLA production, biocatalysis has been explored in the production of a variety of different bioplastics. Polyhydroxyalkanoates (PHAs) or polyhydroxybutyrates (PHBs) have been explored as a bioplastic due to their biodegradability, biocompatibility, and ability to be produced from renewable feedstocks [42] [43] [44]. However, like PLAs above, PHAs and PHBs

also suffer from increased manufacturing costs in comparison to petroleum-derived plastics. PHAs have a higher price range ($US 5-12/kg) than comparable polypropylenes ($US 1.40/kg) [45] [46]. PHBs are produced by fermentation, similarly to PLAs, and the enzymes driving this production have been studied and have been the subject to improvement from many groups. Hori *et al.* [45] have recently done work to improve the production of poly[(R)-2-hydroxybutyrate] through the engineering of the PHA synthase $PhaC1_{Ps}$. Site-directed saturation mutagenesis was used to evolve $PhaC1_{Ps}$ towards improving titers of poly[(R)-2-hydroxybutyrate] (P(2HB)) through production in recombinant *E. coli*. After directed evolution, the group identified $PhaC1_{Ps}$ S325T/S477R/Q481G as being the best protein for P(2HB) production. Through protein modeling, they speculate that this is in part due to the 477R and 481G mutations being positioned where the product exits the active site after catalysis. They theorize that the resulting amino acids may be interacting with the polymer chain. In a similar vein, Normi *et al.* [47], showed improved poly(3-hydroxybutyrate) synthesis via the G4D substitution in *Ralstonia eutropha* type I polyhydroxyalkanoate synthase ($PhaC_{Re}$). This group used *in vitro* evolution by suppression-type mutagenesis that was first pioneered a year earlier by the same group [49] that utilizes an initial "suppressed" mutant of $PhaC_{Re}$ with decreased activity as a starting point to then generate a secondary mutant that has activity gain beyond the wild-type. This is necessary for polyhydroxyalkanoate synthases due to the nature of expression *in vivo*. When synthesized in cells, PHB accumulates within the cell and can make up to 80% of *E. coli* cytoplasm content under optimal conditions. With such a high accumulation, improvements from this starting point are difficult to identify *in vivo*. From the initial mutant scaffold (coined "E11" $PhaC_{Re}$ with a S80P mutation), error-prone PCR was performed and the mutant E11-4 was identified and further characterization showed three amino acid changes that conferred 2-fold higher PHB levels compared to E11: G4D, N208D, and F396L. Further investigation revealed that the G4D mutation was responsible for the higher accumulation of G4D. Both of these enzyme improvement efforts underscore the importance of enzymes and their improvement in the synthesis of bioplastics.

The generation of synthetic fibers for fabrics has also been the subject of bioplastic development. Adipic acid is one of the most important synthetic fiber precursors as it is used in the production of nylon-6,6 [50]. As one of the most abundant synthetic fibers in the world, nylon is traditionally synthesized from adipic acid that has been derived from petrochemically-derived

benzene. As materials generated from adipic acid are common, the production of adipic acid is ripe for targeting through green chemistry. Many groups have investigated the production of adipic acid from renewable sources. Through extensive metabolic engineering, Yu *et al.* [51] were able to design a pathway for the full biosynthesis of adipic acid in recombinant *E. coli* by reverse engineering its degradation pathway, starting from glucose. Taking a step further from a simple sugar to lignin, Niu *et al.* [52] reported an engineered *Pseudomonas putida* strain that utilized aromatic compounds derived from lignin degradation as input into a designed pathway for the biosynthesis of adipic acid. The group used a combination of native and recombinantly expressed enzymes to synthesize adipic acid and this publication was the first to report direct adipic acid production from lignin depolymerization aromatics.

In terms of enzyme engineering, the biosynthetic pathway towards adipic acid has many candidates that can be improved. Saez-Jimenez *et al.* [53] used a variety of different mutagenesis techniques to engineer a (R)-2-hydroxyglutarate dehydrogenase (Hgdh) towards improved 2-oxoadipate reduction. The group focused on a bottleneck in the conversion of (S)-lysine to adipic acid in 2-oxoadipate reduction. The team combined computational analysis and saturation mutagenesis to generate two variants, V11M and V11K, that displayed increased activity on 2-oxoadipate. They then went on to utilize error-prone PCR to further enhance Hgdh activity through A206V/T and A214V/D mutations. In total, the group effectively combined rational engineering strategies and random mutagenesis to develop a highly improved enzyme for generating adipic acid. Along with improvement of existing enzymes, work is also ongoing on discovering new enzymes for the biosynthesis of adipic acid. One of these enzymes was discovered in an enoate reductase from *Clostridium acetobutylicum*. Joo *et al.* [54] showed the conversion of both *cis,cis*- and *trans,trans*-muconic acid to adipic acid by the enoate reductase ER-CA. Previous studies showed *cis,cis*-muconic acid can be produced from biosynthetic pathways as demonstrated in *Escherichia coli* [55], *Saccharomyces cerevisiae* [56], and *Klebsiella pneumoniae* [57] but the hydrogenation to adipic acid remained a challenge once *cis,cis*-muconic acid was produced [50]. Enoate reductases and other ene-reductases have been explored as a solution to this and many more hydrogenation challenges.

1.3 Ene-reductases and Old Yellow Enzymes

1.3.1 History and Characteristics of Old Yellow Enzymes

Ene-reductases perform a simple but exploitable reaction. Members of this enzyme family catalyze the asymmetric hydrogenation of an electron-poor alkene [58] [59] [60]. This enzyme family contains a variety of subclasses including enoate reductases and, importantly for this project, Old Yellow Enzymes (OYEs). First discovered in 1933 [61], the first member of the class that came to be known as OYE1 was the first example of a flavoprotein. Two years later [62], it was elucidated that the yellow character of the enzyme was due to flavin mononucleotide (FMN). OYEs would remain of low interest before the advent of more robust biochemical and molecular biology tools reinvigorated interest in OYEs. Spearheaded since the 1990s by the Massey group, more and more OYEs have been discovered across a wide variety of organisms from higher plants, e.g., *Solanum lycopersicum* (previously *Lycopersicon esculentum*) [63], to cyanobacteria, e.g., *Chroococcidiopsis thermalis* [64], to *E. coli* [65]. As oxidoreductases, OYEs are dependent on a NADH or NADPH cofactor, depending on the enzyme in question. It is through the action of this cofactor and the noncovalently-bound FMN that the catalytic mechanism of OYEs takes place [66]. Common to all OYEs, FMN is nestled within the protein structure and is responsible for the bi-bi ping pong catalytic mechanism of OYEs in which both the reductive and oxidative substrates bind within the same active site [67]. The catalytic cycle of OYEs proceeds in two distinct steps: the reductive half reaction and the oxidative half reaction. As shown in Figure 1, the reductive half reaction utilizes the NAD(P)H cofactor as an electron donor to reduce FMN to $FMNH_2$. Once reduced, the $FMNH_2$ then donates the electrons to the electron poor alkene resulting in an

asymmetric hydrogenation and the creation of two chiral centres. This hydrogenation proceeds in a *trans* addition of the two hydrogens [68].

While this catalytic mechanism remains the same for all OYEs, the function of these enzymes in any given organism varies and the physiological roles OYEs play were not elucidated until long after the prototypical enzyme OYE1 was first discovered. The role for OYE1 in its native *Saccharomyces pastorianus* remains elusive [69] [70], however the roles of other OYEs have been resolved. YqjM, a "thermophilic-like" OYE from *Bacillus subtilis* has been shown to be involved in the oxidative stress response as it is induced in the presence of hydrogen peroxide [71]. Similarly, OYE2 and OYE3 from *S. cerevisiae* have been shown to be involved in the mitigation of reactive oxygen species [72]. Counterintuitively, OYE2 plays a role in both the inhibition and induction of programmed cell death in *S. cerevisiae*. Forming a homodimer of two OYE2 subunits shows an inhibitory effect to programmed cell death while forming a heterodimer with OYE3 enhances cell death and sensitizes cells to oxidative damage. OYE2 has also been implicated in *S. cerevisiae* resistance to acrolein, a toxic by-product of lipid peroxidation [73]. Beyond stress responses, OYEs have also been implicated in carbon and nitrogen use. Pentaerythritol tetranitrate reductase (PETNR) has been shown to be involved in nitrogen utilization by *Enterobacter cloacae*. *E. cloacae* was able to utilize pentaerythritol tetranitrate as a sole nitrogen source and part of this utilization is due to PETNR [74] [75] [76]. Morphinone reductase (MR) is directly involved in the biosynthesis of hydromorphone and hydrocodone from morphinone and codeinone, respectively. This mechanism is used by *Pseudomonas putida* to degrade morphine and codeine and utilize
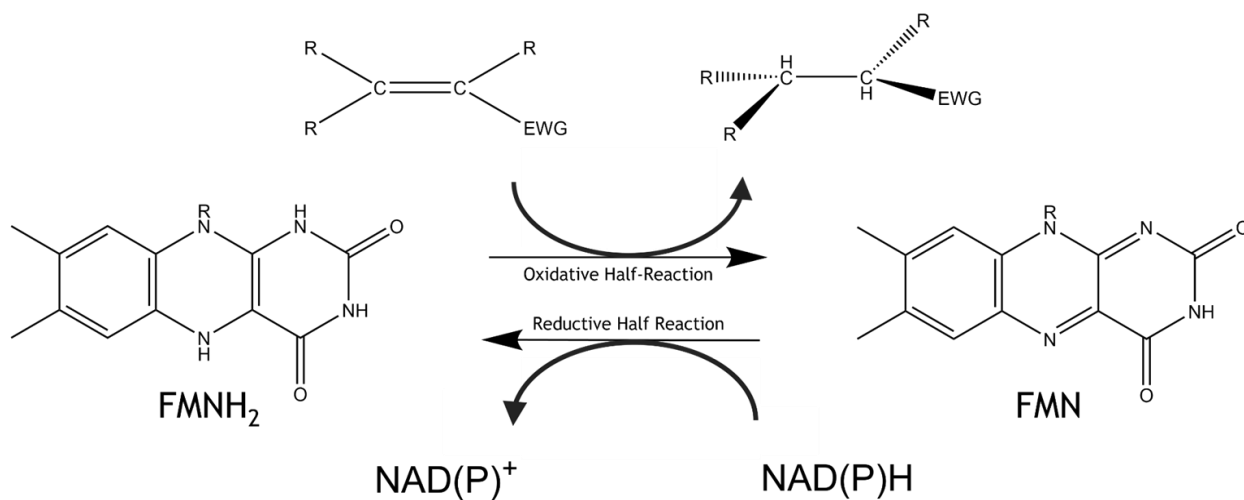
Figure 1: The catalytic cycle of Old Yellow Enzymes.

morphine and/or codeine as a primary carbon source [77] [78] [79]. Finally, OYEs have also been shown to be important in many plants for the production of jasmonic acid, a wound response hormone necessary for regulating defense against herbivores and infections [80] [81]. OPR3 from the aforementioned *S. lycopersicum* has been shown to reduce 12-oxophytodienoic acid in the pathway towards jasmonic acid. Taken together, OYEs have a wide variety of physiological functions and substrates in their native organisms, all being reduced through a shared mechanism across the family.

The OYE family is currently divided into three classes based on phylogenetic analysis. Class I contains the "classical" OYEs from plants and bacteria, class II contains the "classical" OYEs from fungi alone, and class III contains the "thermophilic-like" OYEs [83]. Evolutionarily, class III is much more distinct from class I and II which are more similar to each other. Indeed, before reclassification by Scholtissek et al. [83], there was no distinction between class I and II and OYEs were separated into the "classical" and "thermophilic-like" OYEs [84]. The exemplar of class III is YqjM, which was unique among OYEs at the time of its discovery due to its quaternary structure as a dimer of active dimers (forming a tetrameric structure) and an "arginine finger" that extends from one monomer into the substrate binding site of its partner [71] [85]. This arginine finger is conserved amongst almost all of the class III OYEs and is the major feature that makes class III OYEs distinct within the family [86] [87] [88]. Arginine fingers are not unique to OYEs and have been shown in GTPases [89] and ATPases [90]. In class III OYEs, the arginine finger is thought to be directly involved with substrate recognition as the arginine residue directly interacts with and helps position the substrate in the active site [85].

1.3.2 Old Yellow Enzymes as Industrial Biocatalysts

In efforts to move away from the use of precious metal catalysts to perform *trans*-hydrogenation reactions, ene-reductases and OYEs have been investigated in a variety of biotechnological applications through the lens of green chemistry. As stated above, enzymes provide an avenue to perform these hydrogenations in a more sustainable manner. In the case of OYEs, their large substrate range within the family and their substrate promiscuity in individual enzymes make them an attractive target for industrial biocatalysis [60] [68] [75] [84]. Due to their broad substrate range, OYEs have seen extensive investigation in making chiral building blocks towards valuable products [91]. In pharmaceuticals, a variety of OYEs have been used to generate

(*R*)-profen derivatives, such as (*R*)-flurbiprofen, which have promise as therapeutics for Alzheimer's disease [92] [93]. OYE1, OYE2, and OYE3 have been shown to generate highly enantiomerically-pure methyl (*S*)-2-bromobutanoate, an intermediate in the synthesis of drugs to treat non-insulin-dependent type-2 diabetes [94]. Casting a wide net, Stueckler *et al.* [95] showed the biosynthesis of (*R*)-3-hydroxy-2-methylpropanoate ('Roche Ester') via a variety of OYEs including OYE1/2/3, YqjM, and OPR1. Roche ester and its derivatives are valuable in the synthesis of a number of different compounds including the antibiotics calcimycin [96] and rapamycin [97].

Beyond pharmaceuticals, the chiral building blocks OYEs produce are valuable in a wide variety of other industries. In the fragrance industry, the chirality of compounds is paramount as stereochemical configuration has a large effect on a fragrance's perceived smell [98]. With their robust stereoselectivity, enzymes are valuable to the fragrance industry as catalysts, with OYEs being no exception. Brenna *et al.* (2015) used OYE2 in an enzymatic cascade towards the fragrance molecule 3-methyl-4-pentanolide [99]. NemR-PS, an OYE from *Providencia stuartii*, was engineered to reduce a racemic mixture of neral and geranial to (*S*)-citronellal for the production of (*S*)-citronellol, a raw material important for the selective synthesis of (-)-*cis*-rose oxide [100]. This isomer of rose oxide is the most valuable and is prized for high-end perfumes [101]. Even beyond fragrances, OYEs have been shown in the biosynthesis towards biofuels via YqjM [102], insect pest control pheromones via OYE2.6 [103], and the biobased solvent dihydrolevoglucosenone (Cyrene) via OYE2.6 [104].

While OYEs can add value and reduce reliance on unsustainable traditional chemistry in many applications, important to this work is the biosynthesis of bioplastics via OYEs and other ene-reductases. Of note are four biosynthesis pathways towards bioplastics that ene-reductases play a role, shown in Figure 2.

Illustrated in Figure 2A, *Zhang et al.* (2016) showed the biosynthesis of (-)-β-methyl-δ-valerolactone ((-)MVL) via OYE2 [105]. First a biosynthetic pathway towards mevalonate was established in *E. coli* using glucose as a starting material. Once produced, mevalonate was then converted to anhydromevalonolactone (AMVL) via acid-catalyzed dehydration. AMVL was then hydrogenated to (-)MVL by an OYE2-catalyzed reduction, yielding optically pure material. δ-lactones have garnered interest as biodegradable polyesters. The pathway described by this group also renders these bioplastics biorenewable and fully enzymatically-derived, other than the acid dehydration [106] [107] [108]. Indeed, the group was able to polymerize the enzymatically-derived
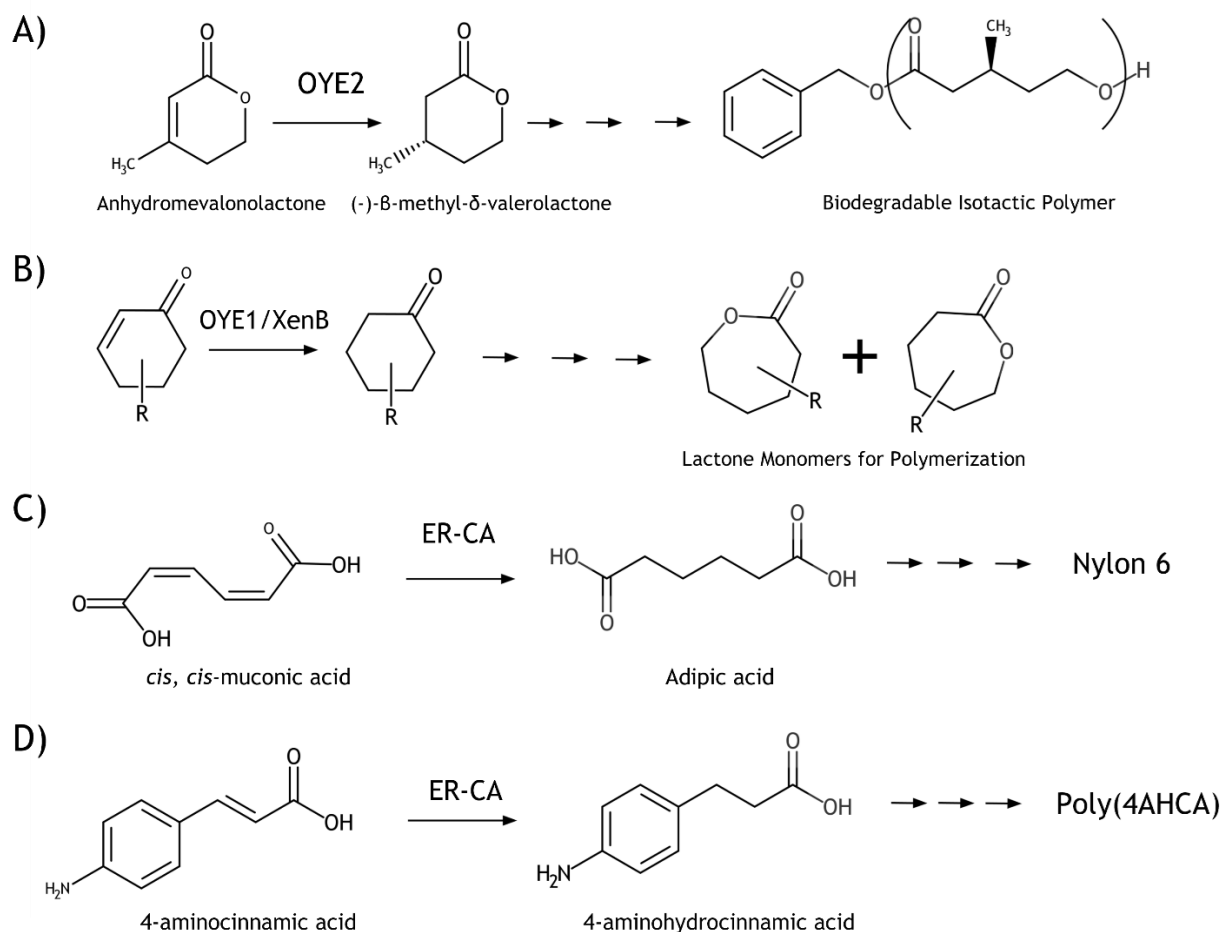
Figure 2: Outline of Biopolymer Precursor Synthesis via Ene-Reductases (Adapted from Toogood and Scrutton [59]).

11

(-)MVL into an isotactic, amorphous polyester. The fermentation of the (-)MVL monomers took upwards of 72 hours to generate 0.8 g/L and converted 69% of the given AMVL, highlighting the need for a faster, more efficient enzyme to achieve higher and quicker conversion of AMVL.

Figure 2B depicts part of an enzymatic cascade designed by Oberleitner *et al.* [109] towards the production of lactone monomers for polyester synthesis. The group investigated the reduction of a panel of substrates including three carvones. Starting from carveol, the group was interested in investigating the production of dihydrocarvides which, like (-)MVL above, can be polymerized for biorenewable polyesters [110]. The group utilized the OYEs OYE1 and XenB for the reduction of the substrates, ultimately moving forward with XenB for a functional demonstration of their enzymatic cascade in the utilization of limonene from orange peel [111]. In 2016, the group demonstrated their enzymatic cascade in the production of carvolactone, another monomer for polyester synthesis [110]. Staying true to the principles of green chemistry, this was done using orange peel waste and highlights the use of OYEs in the production of biopolymers. However, this functional demonstration only produced 6.5 mg carvolactone/g orange peel (0.65% conversion) highlighting the necessity of improving titers. In comparison, 1,3-propanediol, an increasingly popular polyester, can be generated from petroleum-derived ethylene oxide at a 90% yield. Without improvements in titers, even small-market petroleum-derived polyesters are able to outcompete renewable alternatives [112].

Figure 2C outlines the hydrogenation of *cis,cis*-muconic acid to adipic acid which can be used for the synthesis of nylon, as stated in Chapter 1.2. Similarly to Joo *et al.* [54], Sun *et al.* [113] utilized the oxygen-sensitive enoate reductase ER-CA from *Clostridium acetobutylicum* for the reduction of *cis,cis*-muconic acid. However, as an enoate reductase and not an OYE, the mechanism of reduction relies on FMN, FAD, and a 4Fe-4S cluster within the protein rather than FMN alone [114]. The presence of this iron-sulfur cluster renders the enzyme sensitive to oxygen such that it performs at its best in an anaerobic environment. *In vitro* this can be rectified by purging the solution of oxygen but to generate industrial titers of adipic acid, often *in vivo* methods are preferred, and oxygen tolerance is favourable in those methods, both for the organisms as well as for the enzymes performing the biosynthesis. To alleviate this, Sun *et al.* utilized a microaerobic environment for the production of adipic acid in *E. coli* using ER-CA.

ER-CA was also used for the reduction of 4-aminocinnamic acid (4-ACA) to 4-aminohydrocinnamic acid as suggested in Figure 2D. Kawasaki *et al.* [115] investigated this

reduction towards the polymerization of 4-aminohydrocinnamic acid (4-AHCA) which has been demonstrated as a robust bioplastic through polymerization to polyamides and polyimides [116] [117]. These biobased polymers have been shown to have strong thermo-mechanical performance and high chemical stability [118]. The team [115] developed a biocatalytic pathway in *E. coli* for the generation of 4-AHCA from glucose, making these polyamides and polyimides biorenewable and compatible with green chemistry principles. However, the titers of bioplastics produced from this group and indeed the other groups described in this chapter do not compete with the scale of petrochemically-derived plastics.

1.4 Protein Engineering and OYEs

To act as a suitable replacement to petrochemically-derived plastics, bioplastics must be as robust as traditional polymers but also cost efficient to produce. One area of focus towards improving cost efficiency is in efforts to increase the amounts of bioplastic precursors that can be produced by fermentation and enzymatic catalysis. One way to improve enzyme catalysis is by protein engineering. Protein engineering has long been a method for the improvement of protein function [119]. Initially limited to rational design of well-characterized proteins [120], the field has evolved to incorporate diversity via random mutagenesis [121] and, most recently, the use of computational modeling and prediction to aid towards a given function [122]. OYEs are no stranger to engineering approaches involving each of these strategies to varying degrees [69]. In a rational engineering approach, Walton *et al.* [123] selected OYE1 for the stereoselective reduction of three Baylis-Hillman adducts. Baylis-Hillman adducts are the result of Baylis-Hillman reactions which are three-component reactions between an activated alkene and an electrophilic sp^2 carbon in the presence of a catalyst [124]. Forming a wide variety of functionalized molecules, Baylis-Hillman reactions and their adducts are a useful synthetic chemistry technique in the generation of starting material for biologically active molecules [124]. While previous studies had led them to the conclusion that OYE2.6 was already appropriate for the conversion of these adducts to their desired enantiomer, they also investigated full saturation mutagenesis of OYE1 at Trp116. Trp116 was selected in an earlier study attempting to open up the active site of OYE1 to accept bulkier substrates [125]. This was hypothesized due to Trp116's close proximity to the β-substituents of multiple 2-cyclohexenone substrates. Thinking rationally, the group anticipated that replacing Trp116 with a smaller residue would allow larger substrates to access the active site. This was not

the case and changing Trp116 instead altered the stereoselectivity of OYE1 depending on the residue used to replace tryptophan. While not in line with their original hypothesis, this work represents a fully rational approach to improving OYE1, taking advantage of existing crystal structures and a robust characterization of the first discovered OYE.

Building on this work, Nett *et al.* [126] investigated switching the stereoselectivity of a large panel of OYEs using three substrates. Through sequence alignment, the team identified residues analogous to Trp116 in OYE1 and Cys26/Ile69 in YqjM (identified previously to also switch stereospecificity in YqjM [127]) within their panel of OYEs. They hypothesized that by identifying and switching these analogous residues, they could switch the stereospecificity of each of the OYEs. This was somewhat successful, depending on the enzyme and substrate combination. Of note, the same mutation did not have the same effect on stereoselectivity between substrates. While DrER C40D/I81T switched to produce the (*R*) product of 2-methylcyclohexenone, the same amino acid substitution did not cause a switch with (*S*)-carvone. This work and the work of Walton *et al.* [123] highlights a limitation of rational design in that the expected and desired outcome of an amino acid substitution does not always correspond to what effect a mutation would be predicted to cause.

As an alternative to rational design, random mutagenesis and directed evolution are also used as means to improve or alter protein function. While rational design takes advantage of the knowledge and theory of how a protein functions, directed evolution takes a broader approach and instead relies on the generation of large and diverse libraries of randomly or semi-randomly mutated genes (and their corresponding proteins) linked to an observable output to select a most desired mutant out of a "haystack" of neutral or detrimental mutants [128] [129]. Bougioukou *et al.* [127] utilized a directed evolution approach in their generation of YqjM C26D/I69T, a YqjM mutant with increased activity on known substrates and increased substrate range. The team employed a strategy called Iterative Saturation Mutagenesis which is a semi-rational directed evolution approach that first identifies residues for mutagenesis via structural knowledge and then, over multiple cycles, mutagenizes those residues to develop a library of combinatorial mutants. Importantly for this work and any semi-random or fully random mutagenesis strategy, you must be able to correlate the effect of a mutation on a protein to an observable outcome [130]. For Bougioukout *et al.* (2009) after mutant libraries were made, they relied on biotransformations of a

14

compound poorly converted by wildtype YqjM. After a 20 hour incubation, the conversion of substrate to product was analyzed by automated gas chromatography (GC) and used to correlate to high performing mutants.

Daugherty *et al.* [131] also used automated GC to sift through their library of OYE1 mutants generated using circular permutation. Circular permutation does not depend on the mutagenesis of amino acids but rather rearranges the primary amino acid sequence through covalent (peptide) linkage to shift the N- and C- termini, which can alter the tertiary and quaternary structure of proteins to improve catalytic activity and increase substrate scope [132]. Using this approach, the team identified 70 members of the structurally altered library (cpOYE1s) (about 30% of total library size) that had equal or better activity against the common OYE substrate ketoisophorone compared to wildtype OYE1. Primary library screening was done by first producing each library member with *in vitro* transcription and translation (IVTT) in microtiter plates. After sufficient time, the reaction was stopped and substrate, NADPH, and a NADPH regeneration system were added to each well and the conversion via each cpOYE1 was measured via automated GC. After this primary screen and high-performing cpOYE1 variants were identified, further characterization on additional substrates was performed through automated GC as before and by spectrophotometry. The quantification of OYE activity via spectrophotometry is common and is done via measuring the consumption of the NADH or NADPH cofactor at 340 nm. As the stoichiometry between usage of the cofactor and reduction of the substrate is 1:1, the decrease in absorbance at 340 nm serves as an indicator of product formation [71] [133] [134]. Compared to GC analysis of products, measurement of NAD(P)H oxidation via spectrophotometry requires relatively little expertise, costs less in both reagents and equipment, and is potentially faster depending on the level of automation in both methods. However, GC analysis is more sensitive and stands to identify smaller increments of improvement in protein engineering that may be exploited through further design strategies. With these two commonly used assay techniques, a middle ground that utilizes a high-sensitivity, low-cost, and low barrier to entry would be beneficial to screening efforts for the engineering of OYEs.

1.5 Fluorescence-Based Screening Techniques

Fluorescence-based assays are widely used in screening efforts towards small molecule discovery, protein discovery, and aiding in protein engineering. Fluorescent screening techniques

are valuable due to their high sensitivity and speed and have been successfully used for protein identification and engineering in the past [135]. Mei *et al.* [136] utilized the reaction between *para*-methoxy-2-amino benzamidoxime (PMA) and 1,2-butanediol to screen for novel alcohol dehydrogenases (ADHs) and validated their assay's use in screening for improved variants of a well-characterized ADH, *Thermoanaerobacter brockii* SADH (TbSADH). As ketones are generated by TbSADH, they react with PMA to form the fluorophore dihydroquinazoline, which can be detected at 520 nm. They successfully used this technique to identify a variant of TbSADH with 36% increased conversion of 1,2-butanediol as confirmed by GC analysis. Nevolova *et al.* [137] took advantage of an intrinsic pH change caused by the action of haloalkane dehalogenases to develop a high-throughput assay for identifying new dehalogenases. Focused on sensitivity and reliability, the team utilized the pH decrease caused by dehalogenases to eliminate the fluorescence of the fluorophore 8-hydroxypyrene-1,3,6-trisulfonic acid (HPTS). This fluorescence drop was correlated with dehalogenase activity and was verified by GC. While not utilized for protein engineering, the assay was utilized for the identification of novel dehalogenases with activity on an environmental pollutant and a chemical warfare agent.

Beyond using intrinsic pH changes or chemical catalysis alone towards a fluorophore, enzyme-coupled assays have also been utilized for fluorescent-based assays. To investigate phenylalanine ammonia-lyase (PAL) activity and to develop a method for high-throughput screening of engineered PAL variants, Moisă *et al.* [138] utilized ferulic acid decarboxylase 1 (FDC1) from *S. cerevisiae* to decarboxylate the product of PAL activity. Once decarboxylated, the styrene could be added to a tetrazole fluoroprobe via UV light to "activate" the fluorophore and give a fluorescent signal. Kumagai *et al.* [139] utilized a more complicated enzymatic cascade to detect the inhibition of glycosyltransferases. Using NDP kinase, ATP was consumed to phosphorylate UDP and GDP generated from glycosyltransferase activity, generating ADP. ADP was then shunted into use by ADP-hexokinase to phosphorylate glucose to glucose-6-phosphate. G6P dehydrogenase then dehydrogenated glucose-6-phosphate to glucono-1,5-lactone 6-phosphate. This reaction generated NADPH from NADP$^+$ which diaphorase was able to utilize to convert resazurin to resorufin, a fluorophore with emission at 590 nm. While the assay involves a complex series of moving parts, the team was able to utilize the assay to screen 1280 pharmacologically active compounds in the inhibition of B4GALT1. They identified 12

compounds with good inhibitory activity against B4GALT1 and their efficacy was verified via HPLC, showing the robustness of the enzyme-coupled fluorescence assay. The same team utilized a variation of the same assay in the high-throughput screening of kinase inhibitors [140]. Inhibitors of human kinases are valuable as attractive anti-cancer drug targets [141]. To screen for these inhibitors, ADP generated from kinase activity was again utilized by ADP hexokinase to enable G6P dehydrogenase to generate NADPH for diaphorase use, generating fluorescent resorufin. Similarly to the previous study, the team used this enzyme-coupled assay to identify inhibitors for human kinase CLK1. However, the compound library size was scaled up to include an additional library of 214 106 compounds. Importantly to note, the screening of this library was done in a week and the entirety of the detection reagents cost US$ 2500. After the screen, 12 compounds were identified that significantly inhibited CLK1. The speed, cost, and efficacy of the screen highlights the robustness of the fluorescence-based enzymatic activity assay. To this end, a fluorescence-based, enzyme-coupled assay would be valuable to supplement OYE screening and engineering efforts. This assay could combine the cost-effectiveness and ease-of-use of measuring oxidation of NAD(P)H and the sensitivity of GC analysis.

1.6 Objectives and Project Outline

In my project we focused on developing, optimizing, and utilizing a fluorescence-based activity assay for the measurement of OYE activity against the four biopolymer precursors outlined in section 1.3.2. OYEs represent a promising avenue towards sustainable plastics. However, current enzymatic pathways lack the efficiency and titers of petrochemically-derived plastics. These barriers make a switch to sustainable plastics cost-prohibitive and thus better enzymes are needed to catalyze this paradigm shift. A sensitive, cost-effective fluorescence-based assay for the identification and improvement of OYEs towards the generation of sustainable plastics may help alleviate these barriers. With this goal in mind, this project has two main objectives.

1.6.1 Validation and Optimization of Novel Fluorescence-Based Activity Assay

Central to this project is a novel fluorescence-based activity assay developed in the Kwan Lab. This enzymatic cascade relates the activity of a redox enzyme (in our case, OYEs) to the release of 4-methylumbelliferone through a cascade of enzymatic reactions (Fig. 3). As the redox enzyme converts substrate to product, the oxidation of NADH to NAD$^+$ (or NADPH to NADP$^+$)

allows the glyceraldehyde-3-phosphate dehydrogenase GapA to convert glyceraldehyde-3-phosphate to 1,3-biphosphoglycerate. Phosphoglycerate kinase (PgK) then utilizes 1,3-biphosphoglycerate and adenosine-diphosphate (ADP) to generate 3-phosphoglycerate and adenosine-triphosphate (ATP). This ATP is then used by the β-glucoside kinase BglK to add a phosphate group to 4-methylumbelliferyl b-D-glucopyranoside (4MU-Glc), which contains our fluorophore of interest. The fluorophore is then cleaved from the phosphorylated sugar by the 6-phosphoglucoside-specific β-glycosidase, BglA-2. The fluorophore 4-methylumbelliferone (4-MU) can then be measured with excitation at 372 nm and emission at 445 nm. In totality, this enzymatic cascade couples the activity of redox enzymes to 4-methylumbelliferone fluorescence increase.

One of the main goals of this project is to validate and optimize this fluorescence-based activity assay towards the identification of OYEs for sustainable plastic biosynthesis. To this end, this work demonstrates validation of the assay through commercial malate dehydrogenase, characterization of the assay through assessment of Z' (also Z-factor), and optimization of the assay through modification of the glyceraldehyde-3-phosphate dehydrogenase GapA and tuning of cofactor NADPH concentrations.

1.6.2 Screening of OYEs for Activity on Bioplastic Precursors

To demonstrate the applicability of the aforementioned fluorescence-based activity assay, a group of nine diverse OYEs were selected to probe for activity on the four bioplastic precursors shown in section 1.3.2. The nine OYE candidates span the three classes of OYEs and have a wide diversity of sequence similarity (Table S1), structure, substrate range, and host organisms (Table 2). Each OYE was purified and verified as functional within the fluorescence-based activity assay. Once verified, the OYEs were screened against the bioplastic precursors and hits were confirmed by secondary screening and LC-MS.

Table 2: OYE Candidates for Screening

Old Yellow Enzyme	Source Organism	Class
nemA	*E. coli*	I
OPR1	*Solanum lycopersicum*	I
PETNR	*Enterobacter cloacae*	I
OYE1	*S. pastorianus*	II
OYE2	*S. cerevisiae*	II
OYE3	*S. cerevisiae*	II
YqjM	*Bacillus subtilis*	III
RmER	*Cupriavidus metallidurans*	III
DrER	*Deinococcus radiodurans*	III

Chapter 2 - Methodology

2.1 - General Protein Expression and Purification

General protein expression and purification began with the inoculation of a 10 mL pre-culture of Terrific Broth (TB), containing the appropriate antibiotic, with a single colony of a BL21(DE3) *E. coli* strain containing a plasmid encoding the protein of interest. This culture was incubated overnight at 37 °C with shaking.

The next day 8 mL of pre-culture was used to inoculate two 2L Erlenmeyer flasks, each with 396 mL of TB containing the appropriate antibiotic (1% inoculum). Culture was incubated at 37 °C with shaking until an OD of 0.6-0.8 was reached at which time IPTG was added to a final concentration of 0.5 mM. After IPTG addition, cultures were incubated overnight at 18 °C with shaking.

The next day cultures were centrifuged (10 000 × g, 15 minutes, 4 °C) and the supernatant was decanted off. Cells were suspended in 10 mL of wash buffer (50 mM Tris, 500 mM NaCl, 10 mM imidazole, pH 7.5) and lysozyme, DNase I, RNAse A were added each to a final concentration of 5 μg/mL. One Roche protease inhibitor tablet was dissolved in distilled water and added to the cell suspension. Cells were lysed by sonication on ice (25% amplitude, pulse on for 5 seconds, pulse off for 15 seconds, total pulse time 3 minutes) and lysed cells were pelleted by centrifugation (15 000 × g, 30 minutes, 4 °C). Supernatant was recovered and filtered through a 0.22 μm filter.

Supernatant was loaded onto a 1 mL Ni-NTA resin, pre-equilibrated with 10-20 column volumes (CVs) of wash buffer. Once supernatant was loaded onto the Ni-NTA resin, column was washed with 10 CVs of wash buffer. Protein was then eluted with a linear increasing gradient of elution buffer (50 mM Tris, 500 mM NaCl, 300 mM imidazole, pH 7.5) over 30 1 mL fractions. Samples containing protein of interest were kept at 4 °C overnight.

The next day, fractions containing the protein of interest were pooled and concentrated using a Vivaspin 6 or 20 with appropriate molecular weight cutoff (50% of protein's size). Concentrated protein solution was then desalted using an Econo-Pac 10DG desalting column pre-equilibrated with storage buffer (50 mM Tris, 150 mM NaCl, pH 7.5) according to the manufacturer's minimum dilution protocol.

2.2 - Purification of YqjM

The general purification protocol described above rendered YqjM non-functional. The altered purification of YqjM aligned with the general expression protocol up to the resuspension of the cell pellet in Wash Buffer. Alternative Wash (20 mM potassium phosphate, 30 mM Imidazole, pH 6.53), Elution (Elution Buffer: 20 mM potassium phosphate, 250 mM Imidazole, pH 6.53), and Storage (Storage Buffer: 20 mM potassium phosphate, pH 6.53) buffers were used and 5 mM FMN was added to the filtered cell lysate containing YqjM before loading onto the Ni-NTA column. The filtered lysate was then incubated on ice for 50 minutes. In addition, 20 CVs of column washes were performed before elution as opposed to 10.

2.3 - Amplification of OYE2 from *S. cerevisiae* Genomic DNA

The gene encoding Old Yellow Enzyme 2 (OYE2) was PCR-amplified from *S. cerevisiae* genomic DNA (gDNA) for later protein expression and purification. *S. cerevisiae* gDNA extracted from overnight culture of CenPK S. cerevisiae using MasterPure Yeast DNA Purification Kit according to manufacturer instructions. Forward (5'-TGCCGCGCGGCAGCCATATGCCATTTGTTAAGGACTTTAAGC-3') and reverse (5'-CGGAGCTCGAATTCGGATCCTTAATTTTTGTCCCAACCGAGTTTT-3') were designed to flank the coding sequence of OYE2. OYE2 was amplified from the gDNA using Phusion polymerase. PCR amplification product was electrophoresed on 0.6% agarose gel to confirm appropriate amplification. Amplified OYE2 was then gel extracted using EZ-10 Spin Column DNA Gel Extraction Kit (BioBasic).

2.4 - Amplification of OYE3 from *S. cerevisiae* Genomic DNA

The gene encoding Old Yellow Enzyme 3 (OYE3) was PCR-amplified from *S. cerevisiae* genomic DNA for later protein expression and purification. *S. cerevisiae* gDNA extracted from overnight culture of CenPK *S. cerevisiae* using MasterPure Yeast DNA Purification Kit according to manufacturer instructions. Forward (5'-TGCCGCGCGGCAGCCATATGCCATTTGTAAAAGGTTTTGAG-3') and reverse (5'-CGGAGCTCGAATTCGGATCCTCAGTTCTTGTTCCAACCTAAAT-3') were designed to flank the coding sequence of OYE3. OYE3 was amplified from the gDNA using Phusion polymerase. PCR amplification product was ran on 0.6% agarose gel to confirm appropriate amplification. Amplified OYE3 was then gel extracted using EZ-10 Spin Column DNA Gel

Extraction Kit (BioBasic).

2.5 - Cloning of OYE2 or OYE3 into pET28a(+)

OYE2 or OYE3 was cloned into a pET28a(+) backbone using the same modified "SLiCE" method [142]. pET28a(+) was first linearized using BamHI and NdeI and purified using an EZ-10 Spin Column PCR Products Purification Kit (BioBasic). Once purified, linear pet28a(+) was incubated in a 1:3 vector:insert molar ratio along with SLiCE extract and buffer at 37 °C for 15 minutes. Afterwards the SLiCE reaction mixture was transformed into either DH10b or BL21(DE3) *E. coli* via heat shock transformation for genetic manipulation or protein expression, respectively.

2.6 - Fluorescence-Based Activity Assay

The fluorescence-based, NAD(P)H-dependent enzymatic assay was used to assess OYE activity on substrates by measuring the increase in fluorescence of 4-methylumbelliferone (4-MU). Each assay was performed in 50 µL volumes composed of a final concentration of $1\times$ PBS (pH 7.2), 1 mM $MgCl_2$, 1 mM 4-MUGlc, 1 mM glyceraldehyde-3-phosphate (G3P), 0.1 mM adenosine diphosphate (ADP) and 0.02 mg/mL each of GapA, PgK, BgIK, and BgIA-2. Depending on conditions, each assay also contained (+)/(-) 1-2 mM NADPH, (+)/(-) 1 mM substrate (either 2-cyclohexenone, anhydromevalonolactone, S-(+)-carvone, *cis, cis*-muconic Acid, or 4-aminocinnamic acid in equimolar NaOH), and 0.1 mg/mL of the OYE of interest. Each assay was incubated at 37 °C for up to 16 hours, with ongoing fluorescence measurements at 445 nm.

2.7 - Optimization of NADPH Concentration for Fluorescence-Based Activity Assay

Due to the substantial fluorescence observed in reactions containing Class III OYEs but no substrate, optimization of NADPH concentrations was done to ablate off-target fluorescence. Reactions contained 1X PBS (pH 7.2), 1 mM $MgCl_2$, 1 mM 4-MU-Glc, 0.1 mM ADP, 0.02 mg/mL each of 0.02 mg/mL each of GapA G188T P189K, PgK, BgIK, and BgIA-2, 0.1 mg/mL RmER, 1 mM 2-cycohexenone. To these, varying concentrations of NADPH were added. Reactions were incubated at 37 °C for 5 hours with fluorescence measured at 445 nm every minute.

2.8 - Verification of Optimized Conditions in Fluorescence-Based Activity Assay with All

OYE Candidates

Optimized assay conditions were tested with all 9 OYE candidates. Each reaction contained 1X PBS (pH 7.2), 1 mM $MgCl_2$, 1 mM 4-MU-Glc, 0.1 mM ADP, 0.02 mg/mL each of GapA G188T P189K, PgK, BglK, and BglA-2, (+)/(-) 2 mM NADPH, (+)/(-) 1 mM 2-cyclohexenone, and 0.1 mg/mL OYE of interest. Reactions were incubated at 37°C for 2 hours and fluorescence was measured at 445 nm every 2 minutes.

2.9 - Site-Directed Mutagenesis of GapA

Mutations were introduced into gapA through PCR-mediated site-directed mutagenesis. Two residues were altered: G188T and P189K. Forward (5'-CAGAAAACCGTTGATACCAAGTCTCACAAAGACTGG-3') and reverse (5'-CCAGTCTTTGTGAGACTTGGTATCAACGGTTTTCTG-3') primers were designed to amplify the mutant GapA (GapA G188T P189K) from an existing pET28a(+)-GapA construct through PCR. Mutagenic primers were used in conjunction with sense (5'-GCTGGACGCGGATGAACAGGCAGACATCTG-3') and antisense (5'-CAGATGTCTGCCTGTTCATCCGCGTCCAGC-3') primers to the ROP protein existing in the pET28a(+) backbone. Mutant forward primer was used with the ROP sense primer and the mutant reverse primer was used with the ROP antisense primer. Once both reactions were amplified, PCR products were purified using an EZ-10 Spin Column PCR Products Purification Kit (BioBasic). SLiCE reaction was then performed to ligate the two construct fragments together and the mutant GapA construct was transformed into DH10b and BL21(DE3) *E. coli*.

2.10 - Comparison of Affinity of Wild-type GapA for NAD^+ vs $NADP^+$

The ability of wild-type GapA to utilize $NADP^+$ as opposed to its native NAD^+ was assessed. Each assay consisted of 1X PBS (pH 7.2), 1 mM $MgCl_2$, 1 mM 4MU-Glc, and 0.02 mg/mL each of wild-type GapA, PgK, BgIK, and BgIA-2. Depending on conditions, individual assays contained (+)/(-) 1 mM G3P, (+)/(-) 0.1 mM ADP, and (+)/(-) 1mM $NAD^+/NADP^+$. Reactions incubated at 37C for 10 minutes and fluorescence was measured via plate reader at 445 nm.

2.11 - Comparison of Wild-type and Mutant GapA

Affinity towards NAD^+ and $NADP^+$ was compared between the native and variant GapA. Each assay consisted of 1X PBS (pH 7.2), 1 mM $MgCl_2$, 1 mM 4MU-Glc, and 0.02 mg/mL each of GapA (mutant or wildtype), PgK, BgIK, and BgIA-2. Depending on conditions, individual assays contained (+)/(-) 1 mM G3P, (+)/(-) 0.1 mM ADP, and (+)/(-) 1mM $NAD^+/NADP^+$. Reactions were incubated at 37C for 10 minutes and fluorescence was measured via plate reader at 445 nm.

2.12 - Enzyme Kinetics of OPR1 by Absorbance

Steady state kinetics of OPR1 on S-(+)-Carvone were established by measuring the rate of NADPH oxidation at 340 nm. Assays were performed in 50 µL volumes in a 96 well plate with 1 mM NADPH, varying concentrations of S-(+)-Carvone, and 1.25 µg purified OPR1. Assays were performed in Storage Buffer at 30 °C. Assays were performed under aerobic conditions and NADPH oxidation by molecular oxygen was accounted for.

2.13 - Enzyme Kinetics of OPR1 by Fluorescence

Steady state kinetics of OPR1 on S-(+)-carvone were attempted to be established by measuring the rate of 4-methylumbelliferone release through the fluorescence-based activity assay at an emission at 445 nm. Assays were performed in 50 µL volumes with 1X PBS (ph 7.2), 1 mM $MgCl_2$, 1 mM 4MU-Glc, 0.1 mM ADP, 0.02 mg/mL each of GapA, PgK, BgIK, and BgIA-2, 2 mM NADPH, 20 ng (0.004 mg/mL) purified OPR1, and (+)/(-) varying concentrations of S-(+)-carvone. Assays were performed in Storage Buffer at 30 °C under aerobic conditions. Calculations accounted for fluorescence generated without substrate.

2.14 - Quantification of FMN Content of Protein Purifications

To investigate the cause of the off-target fluorescence, the FMN content of select protein purifications was assessed. The method is modified from Faeder and Siegel [143]. OYE purifications were boiled for 3 minutes and cooled rapidly to separate the FMN from the protein. Once cooled, samples were centrifuged at $20\,000 \times g$ for 10 minutes and supernatant was collected. Supernatant was then measured in 1 cm path length cuvette via absorbance at 450 nm and FMN concentration was calculated using the established extinction coefficient of $12\,200\ M^{-1}\ cm^{-1}$.

Chapter 3 - Results and Discussion

3.1 - A Fluorescence-Based Coupled Enzyme Cascade to Assay NAD(P)H-Dependent Oxidoreductase-Catalyzed Reactions
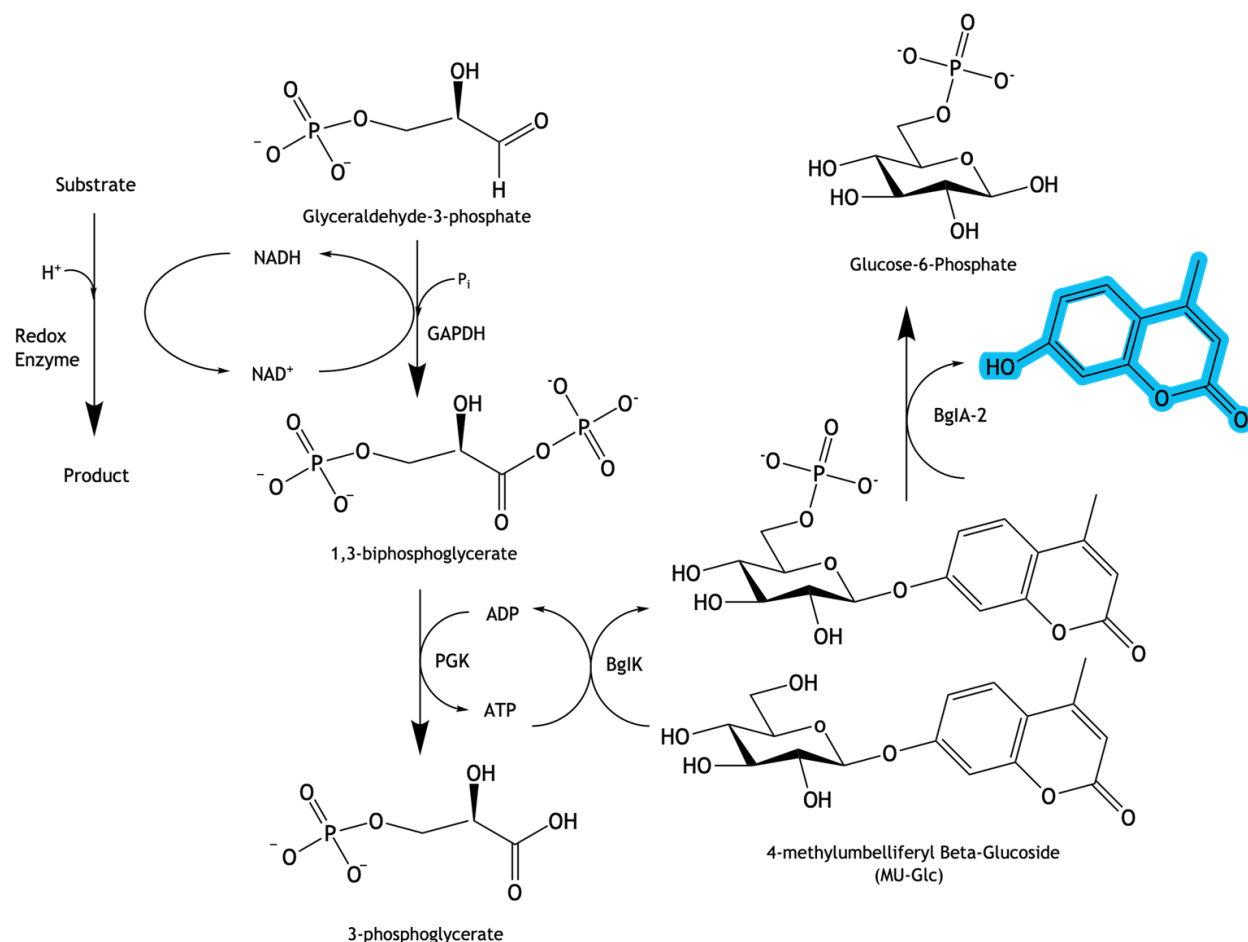
Figure 3. **Outline of the Fluorescence-Based Activity Assay.** Oxidation of NADH to NAD$^+$ leads to the release of 4-methylumbelliferone correlating redox enzyme activity with fluorescence increase.

The ability to screen oxidoreductase activity is important in identifying useful biocatalysts from nature, and also towards engineering novel ones through directed evolution. Many valuable redox enzymes are dependent upon NAD(P)H as an electron donating co-substrate (or conversely, upon NAD(P)$^+$ as an electron acceptor), and the common method to detect their activity is to monitor the change in absorbance at 340 nm as NAD(P)H is converted to NAD(P)$^+$ (or *vice versa*).

In our research group, we have developed a fluorescence-based, enzyme cascade-coupled system to detect oxidoreductase activity with orders of magnitude more sensitivity than conventional absorbance-based assays (Figure 3). While recycling NAD(P)H from NAD(P)$^+$, the coupled enzyme cascade triggers cleavage of a labeled glycoside, releasing a strong fluorescent signal (*via* the fluorophore 4-methylumbelliferone). This allows detection of very low levels of a specific oxidoreductase activity that we may wish to magnify by directed evolution.

Using our screening strategy, NAD(P)H-dependent reductase activity catalyzed by OYEs can be detected through an enzymatic cascade that uses the by-product NAD(P)$^+$ along with glyceraldehyde-3-phosphate and inorganic phosphate in glyceraldehyde-3-phosphate dehydrogenase (GapA)- and phosphoglycerate kinase (PGK)-catalyzed reactions to generate ATP that can be used by a β-glucoside kinase (BglK) to phosphorylate a fluorogenically labeled glucoside, enabling its cleavage by a 6-phospho-β-glucosidase (BglA-2), releasing fluorescence. Initial experiments performed to test this enzymatic cascade showed indeed that fluorescence depended upon NAD$^+$ added to the reaction, along with the presence of the coupling enzymes, GapA, PGK, BglK, and BglA-2, and their substrates (Figure 4).
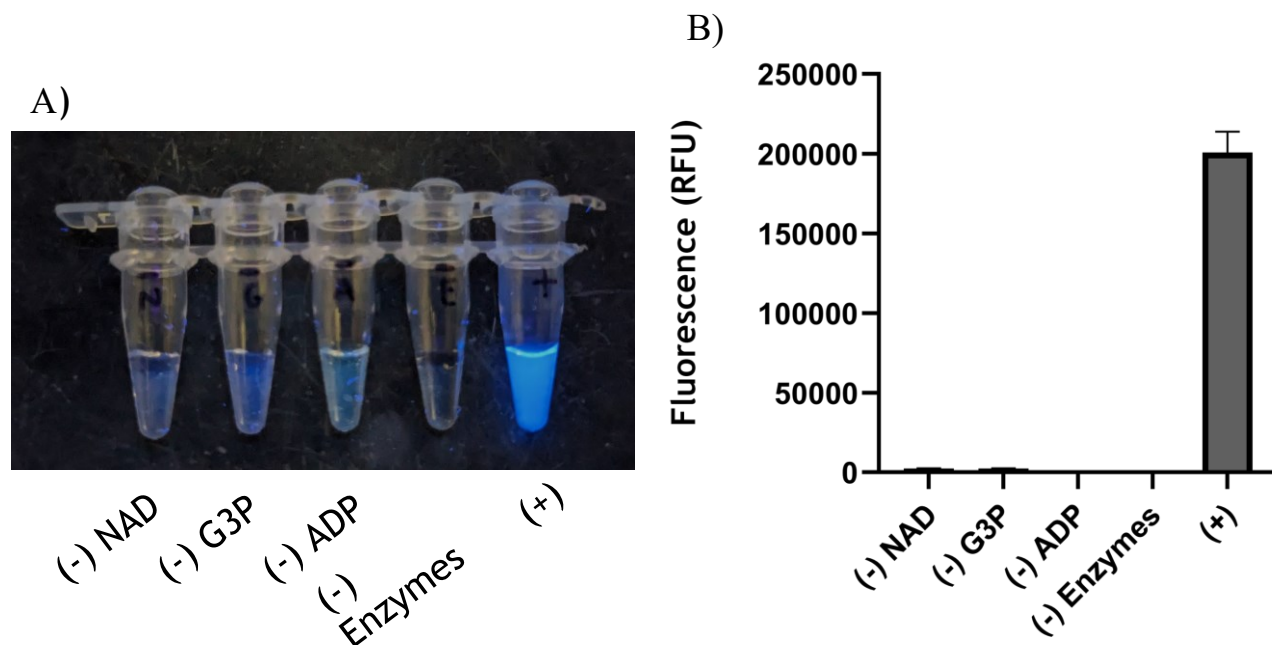
Figure 4: Activity of Fluorescence-Based Activity Assay with Free NAD⁺. Fluorescence-based activity assay was assessed for function without a coupled redox enzyme. Reaction was incubated at room temperature for 5 minutes before visualising fluorescence by illumination under long-wave UV light (Panel A) and quantifying fluorescence at 445 nm (Panel B).

As shown in Figure 4, there is a concerted fluorescence increase both qualitatively and quantitatively when all reaction conditions are present (NAD⁺, G3P, ADP, and supporting enzymes GapA, PGK, BglK, and BglA-2), indicating that the fluorescence-based activity assay proceeds as expected without being coupled to a redox enzyme.

3.2 - Verification of Fluorescence-Based Activity Assay

Before moving to use this coupled enzyme cascade to assay our Old Yellow Enzymes, we next verified that it could be used to detect oxidoreductase activity using a commercially sourced, well-characterized redox enzyme, malate dehydrogenase (from pig heart). Malate dehydrogenase was coupled to the enzymatic cascade together with the addition of its substrate (oxaloacetate) and its NADH cofactor.

As seen in Figure 5, fluorescence increase corresponding to the release of 4-methylumbelliferone only occurs in the reaction with all necessary components (including the redox enzyme malate dehydrogenase, its substrate oxaloacetate, and the cofactor NADH). The

fluorescence increase over 60 minutes verifies the functionality of our fluorescence-based activity assay (Fig. 5).
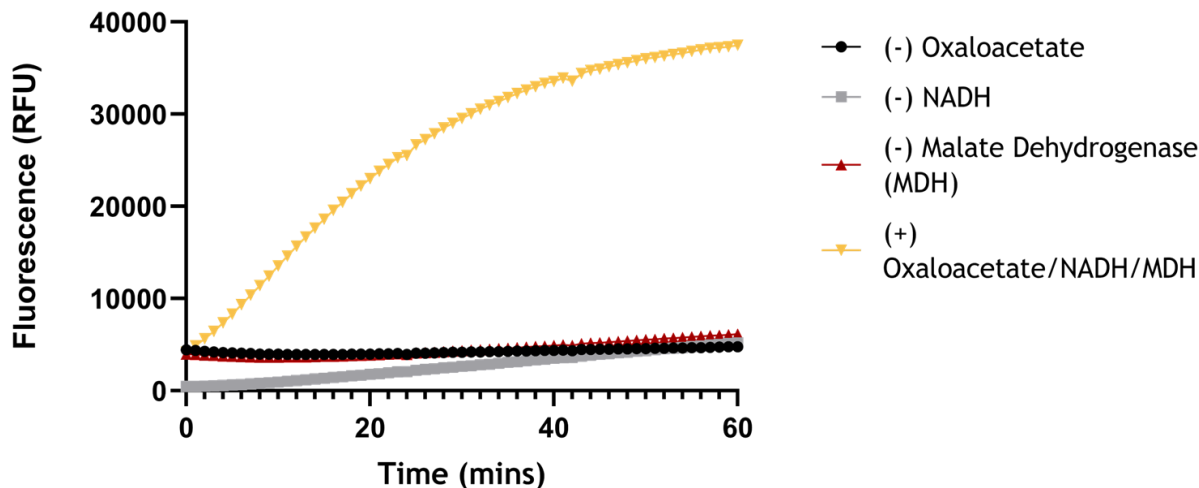
Figure 5. **Activity of Malate Dehydrogenase on Oxaloacetate via Fluorescence-Based Activity Assay**. Fluorescence measured at 445 nm over 60 minutes to verify the function of the Fluorescence-Based Activity Assay.

3.3 - Optimization of Fluorescence-Based Activity Assay: Mutation of GapA

While our initial tests demonstrate that we can detect the NADH-dependent oxidoreductase activity with malate dehydrogenase, many important redox enzymes prefer NADPH as a cofactor over NADH. This is true of many OYEs, including the nine candidate enzymes we chose to study. This posed a challenge because the glyceraldehyde-3-phosphate dehydrogenase from *E. coli* (GapA) that is employed in our coupled enzyme cascade has a strong preference for NAD^+ over $NADP^+$. In order to better adapt the fluorescence-based activity assay to the OYE candidates, the ability of the native glyceraldehyde-3-phosphate dehydrogenase GapA to utilize $NADP^+$ was assessed. This investigation was done to determine the feasibility of adapting the existing coupled enzyme cascade to accommodate the preference of NADPH-dependent OYEs in assaying their activity. A test of the coupled enzyme cascade was started with the addition of either NAD^+ or $NADP^+$ to a reaction containing GapA, PGK, BglK, and BglA-2 along with the necessary substrates for these coupling enzymes. This reaction was allowed to continue for 10 minutes before fluorescence was measured at 445 nm. As shown in Figure 6A, there is a significant fluorescence increase in the reaction containing NAD^+, which is expected. However, there is also a significant increase in fluorescence in the reaction containing $NADP^+$ (although this was of a lower magnitude

28

compared to the reaction containing NAD$^+$) indicating that GapA does have activity with NADP$^+$ as cofactor, albeit to a much smaller degree than it does when NAD$^+$ is the cofactor.
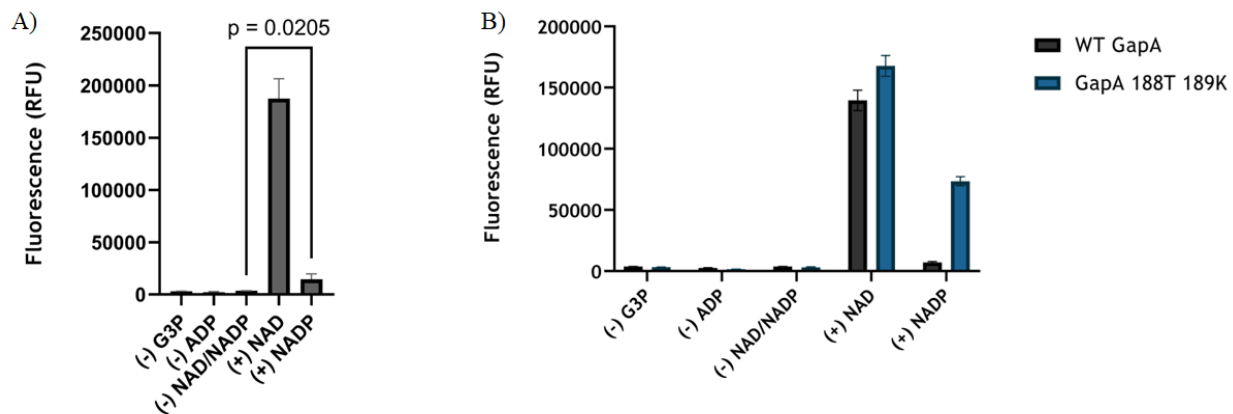
Figure 6. Mutation of GapA for Fluorescence-Based Activity Assay. A) Ability of native GapA to use NADP$^+$. Reaction allowed to continue for 10 minutes at room temperature before measuring fluorescence at 445 nm. B) Comparison of activity of variant GapA and native GapA with NADP$^+$. Reaction allowed to continue for 10 minutes at room temperature before measuring fluorescence at 445 nm.

With this cross-reactivity to NADP$^+$ established, we sought to increase GapA's ability to utilize NADP$^+$ in order to eliminate this potential constraint on the fluorescence-based activity assay. Slivinskaya et al. [147] demonstrated a GapA double mutant (GapA G188T P189K) that showed a significantly higher activity on NADP$^+$ compared to native enzyme. This variant was generated and its activity on NADP$^+$ within the fluorescence-based coupled enzyme cascade was assessed. Reactions were allowed to continue for 10 minutes before fluorescence was measured at 445 nm. Figure 6B shows the stark effect of this double substitution on the fluorescence observed when NADP$^+$ is used as the cofactor within the fluorescence-based activity assay. While activity on NAD$^+$ remains similar, the ability of GapA G188T P189K to utilize NADP$^+$ is significantly increased leading to higher amounts of fluorescence as compared to the native enzyme with the same concentrations of NADP$^+$ present in solution. This change diminishes a potential bottleneck for the assay by reducing the amount of fluorescence that is gated by the activity of GapA which is necessary to optimize the assay to be completely or nearly-completely dependent on the activity of the chosen OYE or another redox enzyme.

3.4 - Expression and Purification of Old Yellow Enzyme Candidates

The nine OYE candidates were each cloned into pET28a(+) vectors. Seven were commercially ordered through Twist Biosciences and were codon optimized for expression in *E.*

coli. The genes encoding OYE2 and OYE3 were amplified from *S. cerevisiae* genomic DNA and the subsequent amplified genes were used for SLiCE [141] cloning into pET28a(+). Each pET28a+OYE constructs were separately transformed into BL21 (DE3) *E. coli* and subsequently expressed and purified using the same general protein purification method where possible. Under these conditions we observed expression of each of the enzymes (as shown in Figure 7) but for YqjM, we were unable to recover fully active enzyme. YqjM is a Class III OYE that has established literature demonstrating robust activity on 2-cyclohexenone [144] and so optimization of YqjM expression and purification was done. Two optimization avenues were pursued: buffer optimization and FMN saturation. For the former, phosphate buffer was used as the base for the wash, elution, and storage buffers instead of the general Tris-HCl buffers. This change was done to more closely mimic the original paper characterizing YqjM [71]. Beyond pH, which can be essential for the function of a protein, buffer composition can also play a role in modulating protein function *in vitro*. Protein-protein interactions, for example, may be strongly influenced by buffer [145] and this can be especially important for the catalytic activity of dimeric enzymes like YqjM. Secondly, following filtration of the cell lysate, the filtered lysate was incubated at 4 °C for 50 minutes with 5 mM FMN. This incubation is often performed when characterizing OYEs [71] [146] and was done in this work to fully saturate every YqjM protein with the FMN cofactor that is crucial for the mechanism of OYEs. Through the combination of these two optimization steps, function was restored to YqjM as demonstrated by results of the coupled cascade assay of OYEs (as further described in the next section, **3.5**) shown in Supplementary Figure A2.
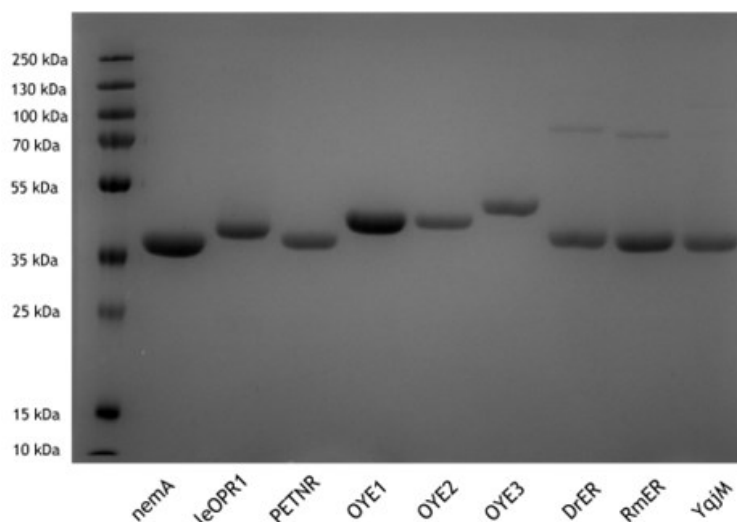
Figure 7. Purification of OYEs and Optimization of YqjM Expression. A) Coomassie Blue-stained SDS-PAGE gel showing the 9 His-tagged OYE candidates after protein purification.

3.5 - Verification of Old Yellow Enzyme Function in Fluorescence-Based Activity Assay

Once purified, the 9 OYE candidates were investigated for functionality. For this purpose, 2-cyclohexenone was used as a substrate since it is commonly used in characterization studies of OYEs and activity on 2-cyclohexenone is widely conserved throughout the different OYE classes [68] [78] [125]. Each OYE was tested for NADPH-dependent reductase activity in the fluorescence-based assay coupled to the enzymatic cascade as illustrated in Figure 3. The assay was performed with 2-cyclohexenone either present or absent. Reactions were incubated at 37 °C for up to 16 hours, with fluorescence readings at 445 nm. We tested OYEs employing either native GapA or the engineered G188T P189K variant (described in 3.3) in the coupled enzyme cascade, and we found that although use of the wild-type GapA permits the detection of OYE activity on 2-cyclohexenone by increased fluorescence relative to controls without 2-cyclohexenone (Supplementary Figure A1), the change in signal is much more pronounced when GapA G188T P189K is used in the cascade. This was demonstrated by comparing the enzyme cascade-coupled assay of the PETNR enzyme with either GapA variant as illustrated in Figure 8.
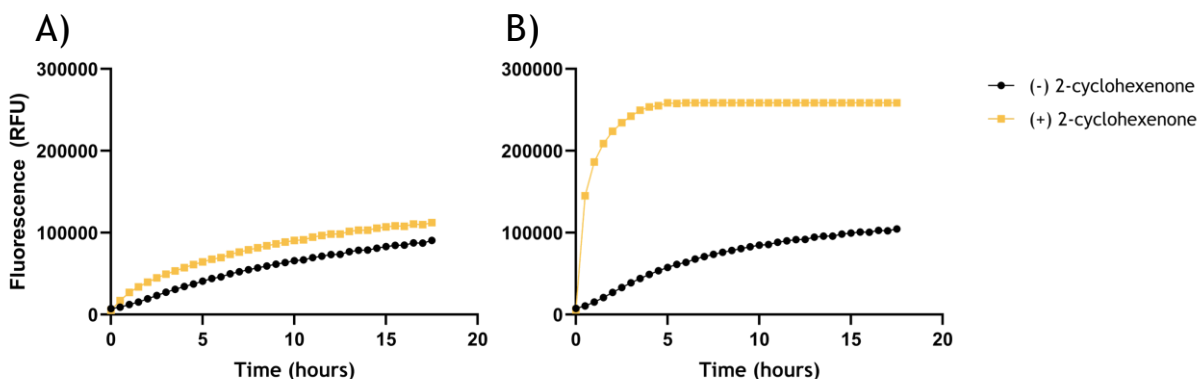
Figure 8. Comparison of PETNR activity within fluorescence-based activity assay using native (panel A) or GapA G188T P189K (panel B). Assay was performed at 37 °C for 16 hours, measuring fluorescence at 445 nm every 30 minutes.

In testing the enzyme cascade-coupled assay optimized for NADPH-dependent reductases (including the mutant GapA G188T P189K), we observed significant off-target fluorescence for Class III OYEs in control experiments that excluded the OYE substrate (2-cyclohexenone), which we hypothesized is due to NADPH oxidation that is independent of such a substrate (*e.g.*, oxidation by molecular oxygen). After optimizing assay conditions (namely NADPH concentrations) to minimize the ratio of signal from negative to positive controls (Appendix A.1 and supplementary Figure A3), we identified optimized conditions using 2 mM NADPH in the enzyme cascade-coupled assay.

Optimized assay conditions containing GapA G188T P189K and 2 mM NADPH were tested with all nine OYE candidates. Activity of each OYE candidate on 2-cyclohexenone was assessed with optimized conditions to reverify the functions of the OYE candidates in the optimized conditions. Figure 9 shows the effect of the optimized conditions on Class I, II, and III OYEs. While nemA and PETNR are not significantly affected by the optimized conditions, the difference between positive and negative controls is greatly enhanced in the OPR1 conditions. The Class II OYEs are similarly unhindered by the optimized conditions. In the Class III OYEs, both YqjM and DrER's off-target fluorescence shown in Figure A1 are dampened by the new optimized conditions, however RmER continues to have high levels of off-target fluorescence. Further optimization through altered purification methods or further adjustment of reaction conditions may be necessary to fully ablate the off-target fluorescence found within the Class III OYEs.
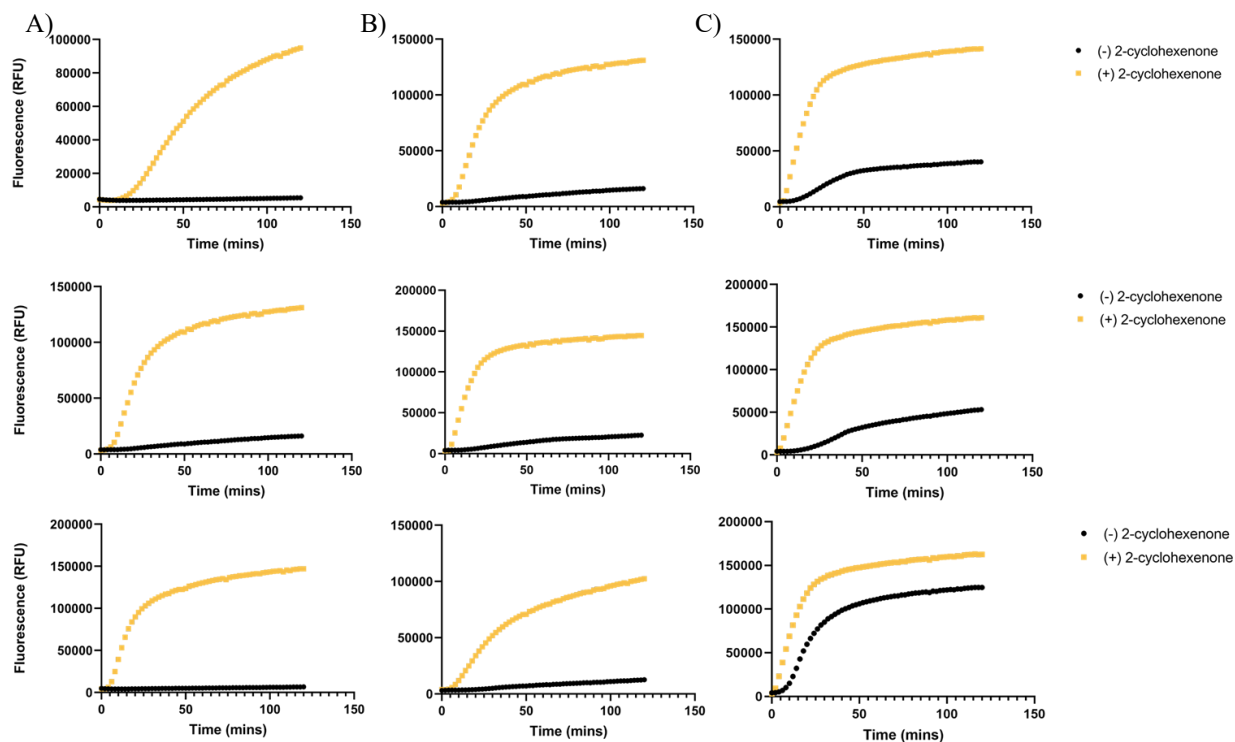
Figure 9. Verification of OYE Function within Fluorescence-Based Activity Assay with Optimized Conditions. A) Verification of Class I OYEs function. In descending order: nemA, OPR1, and PETNR. B) Verification of Class II OYEs function. In descending order: OYE1, OYE2, and OYE3. C) Verification of Class III OYEs function. In descending order: YqjM, RmER, and DrER. Fluorescence measured at 445 nm every 5 minutes for 2 hours.

Prior to carrying out high-throughput screening assays with a variety of OYE and substrate combinations, we further characterized the assay to test its sensitivity and calculate Z' (also Z-factor; not to be confused with Z-score). Sensitivity is one of the advantages of using an enzyme-couple fluorescence-based assay, and the sensitivity of our assay was investigated through different OYE2 concentrations. Z' is a measure of the signal-noise ratio of a high-throughput assay. By measuring the fluorescence of the positive control versus the negative control, Z' will estimate the consistency of the assay with a Z' value of 1 being ideal [148]. OYE2 concentrations varied from 0.1 mg/mL (the concentration used in subsequent screenings) to 0.0004 mg/mL. Activity against 2-cyclohexenone via fluorescence at 445 nm was measured every minute for 180 to 240 minutes.
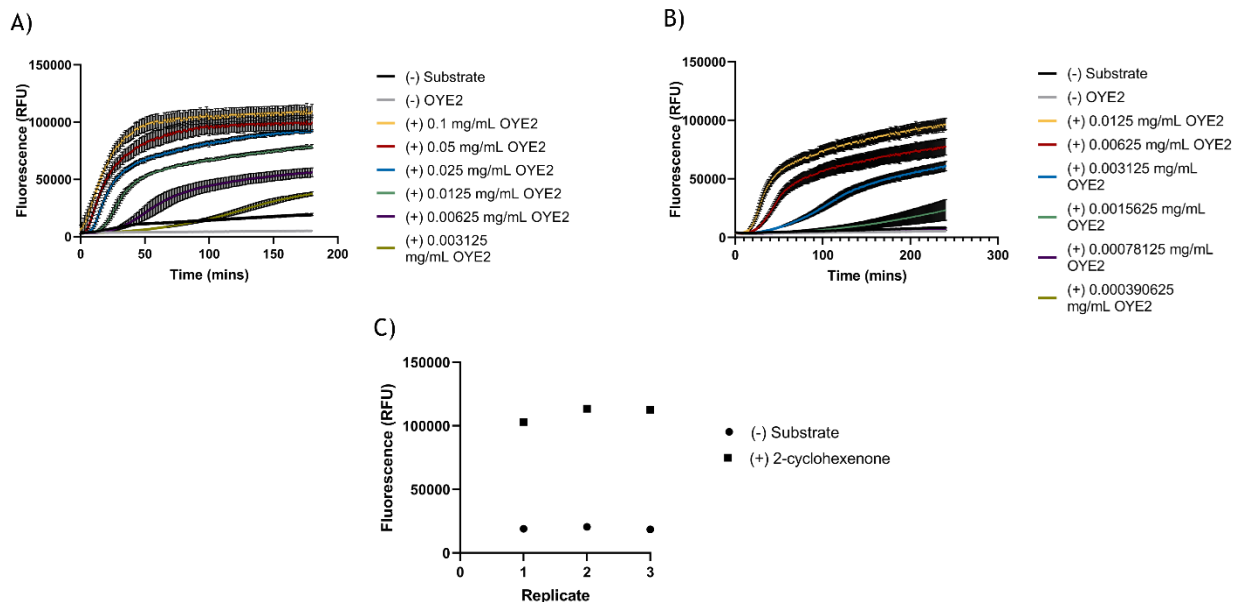
Figure 10: Characterization of Sensitivity and Z' Value of Fluorescence-Based Activity Assay. A) Differing concentrations of OYE2 were assessed for activity on 2-cyclohexenone over 3 hours. B) Differing concentrations of OYE2 were assessed for activity on 2-cyclohexenone over 4 hours. C) Z' value for the assay with 0.1 mg/mL OYE2 was determined to be 0.82 at 180 mins.

In Figure 10A, concentrations from 0.1 mg/mL to 0.003 mg/mL are shown. By the end of the three hours, the 0.003 mg/mL condition is significantly increased in fluorescence as compared to the (-) substrate control ($p = >0.0001$). Figure 10B shows similar results down to 0.0016 mg/mL ($p = 0.0431$), however concentrations of OYE2 lower than this do not show significant fluorescence. This may be due to these concentrations being lower than the limit of detection (LOD) for the assay or may be due to the assay being performed for only four hours. In the last 30 minutes of the assay, the rate of fluorescence generation in the 0.0008 mg/mL condition starts to outcompete the (-) substrate control (25.79 RFU/min vs 23.53 RFU/min, respectively). As the significant 0.0016 mg/mL condition also took about three hours to become significantly different from the negative controls, it's possible that the 0.0008 mg/mL condition will also eventually outcompete the negative control. While further work is required to determine the true sensitivity of the assay, we have demonstrated that enzyme concentrations down to the nM range are able to be detected via this assay. As shown in Figure 10C, Z' was assessed for this assay and was found to be 0.82. This Z' indicates a low amount of variability in the assay in the conditions tested and demonstrates that this assay is potentially viable for high throughput applications as Z' values between 0.5 and 1 are generally considered good [149].

3.6 - Screening of Activity of OYE Candidates Against Biopolymer Precursors

The activity of the nine OYE candidates on the four biopolymer precursors was assessed using the fluorescence-based activity assay. Each set of reactions contained three controls: without NADPH, without substrate, and with the positive control 2-cyclohexenone. The assays were performed over 16 hours at 37 °C and fluorescence readings were taken every 3 minutes at 445 nm. Reactions were done in quadruplicate and a hit was considered positive if the endpoint measurement was significant by an unpaired student's T-test which has been used in high-throughput assays to define hits in the past [150] [151]. The results from the screening are shown in Figures 11, 12, and 13, separated by class. In Figure 11, the results from the screening of the Class I OYEs are shown. The only hit identified for each enzyme within this class is S-(+)-carvone. For each of these enzymes, this is unsurprising as nemA, OPR1, and PETNR are all reported to have activity on S-(+)-carvone [152] [153]. However, this is the first time that these enzymes have been directly compared and thus comparisons of their activities within the context of the fluorescence-based activity assay can be drawn. Within this context, OPR1 has the most robust activity on S-(+)-carvone, outcompeting PETNR and nemA in rate of reaction and amount of fluorescence generated. OPR1's activity on S-(+)-carvone also outcompetes the positive control 2-cyclohexenone. While kinetics on 2-cyclohexenone have not been demonstrated for OPR1 in literature, OPR1 has been shown to have activity on a wide variety of electron-poor alkenes including dicarboxylic acids, dimethyl esters [154], and ketones, including a molecule similar in structure to 2-cyclohexenone: 2-methylcyclohexenone [155]. Despite this, an alternative positive control may be necessary to include for OYE screenings going forward such as ketoisophorone, another molecule subject to widely conserved activity across the OYE classes [155].
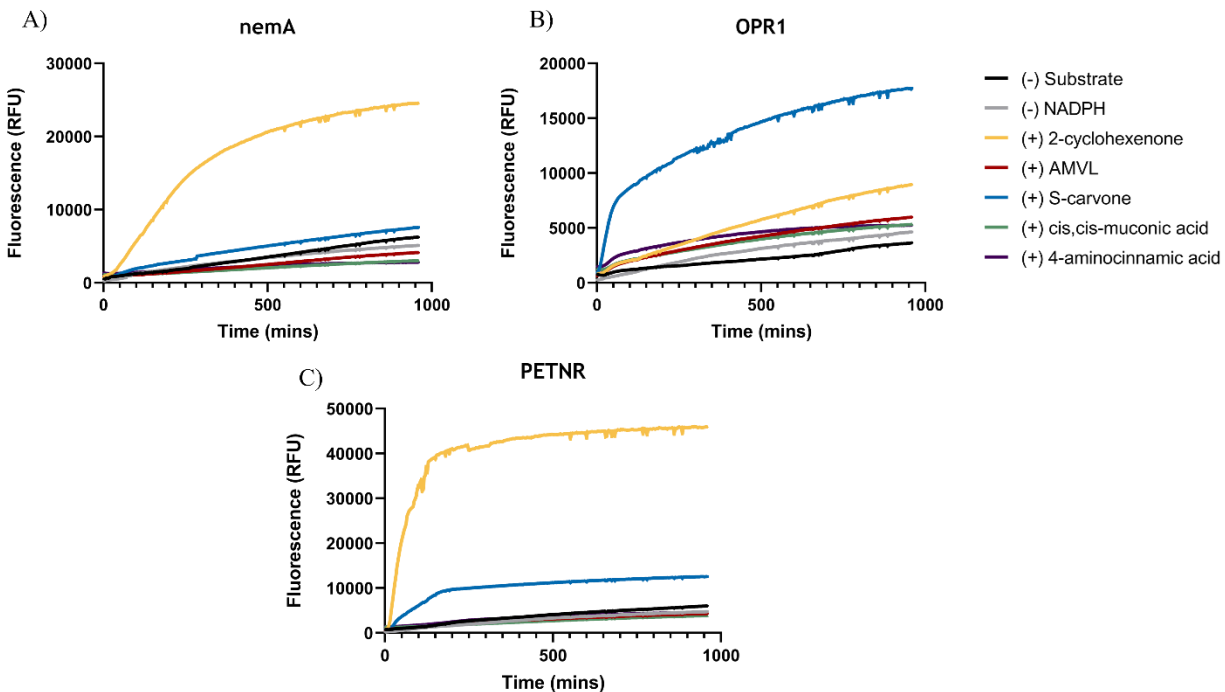
Figure 11. Results of Screening Assay with Class I OYEs. A) Activity of nemA on biopolymer precursors. Assay was performed at 37 °C for 16 hours with fluorescence measurements every 3 minutes at 445 nm. B) Activity of OPR1 on biopolymer precursors. Assay was performed at 37 °C for 16 hours with fluorescence measurements every 3 minutes at 445 nm. C) Activity of PETNR on biopolymer precursors. Assay was performed at 37 °C for 16 hours with fluorescence measurements every 3 minutes at 445 nm.

In comparison to the Class I OYEs in Figure 11, the Class II OYEs exhibit significantly lower activity across the class on any of the biopolymer precursors as shown in Figure 12. Neither OYE2 nor OYE3 show activity on any biopolymer precursors and OYE1 only shows activity on S-(+)-carvone that is statistically significantly higher than the (-) substrate control ($p < 0.05$). OYE1 is expected to have activity on S-(+)-carvone and has been used within the context of generating biopolymers and is shown to convert S-(+)-carvone to dihydrocarvone [109] and has been independently reported to reduce S-(+)-carvone as well as its enantiomer R-(-)-carvone [156]. However, the negative results from OYE2 and OYE3 are unexpected for multiple reasons. Firstly, previous reports in literature have indicated that OYE3 is active both on S-(+)-carvone and its enantiomer [157]. Therefore, we should expect an increase in fluorescence in the reaction containing S-(+)-carvone and OYE3. There may be some activity that is obfuscated by off-target fluorescence found in the (-) substrate control. This may also be the result of outliers found within the screening as discarding the lowest fluorescence outlier for (+) carvone and the highest fluorescence outlier for (-) substrate renders the difference between the two significant by an

unpaired t-test (p = 0.0352), which would indicate a hit and therefore activity. This inconsistency highlights a necessity to further optimize the fluorescence-based activity assay to decrease the presence of outliers and the presence of off-target fluorescence.
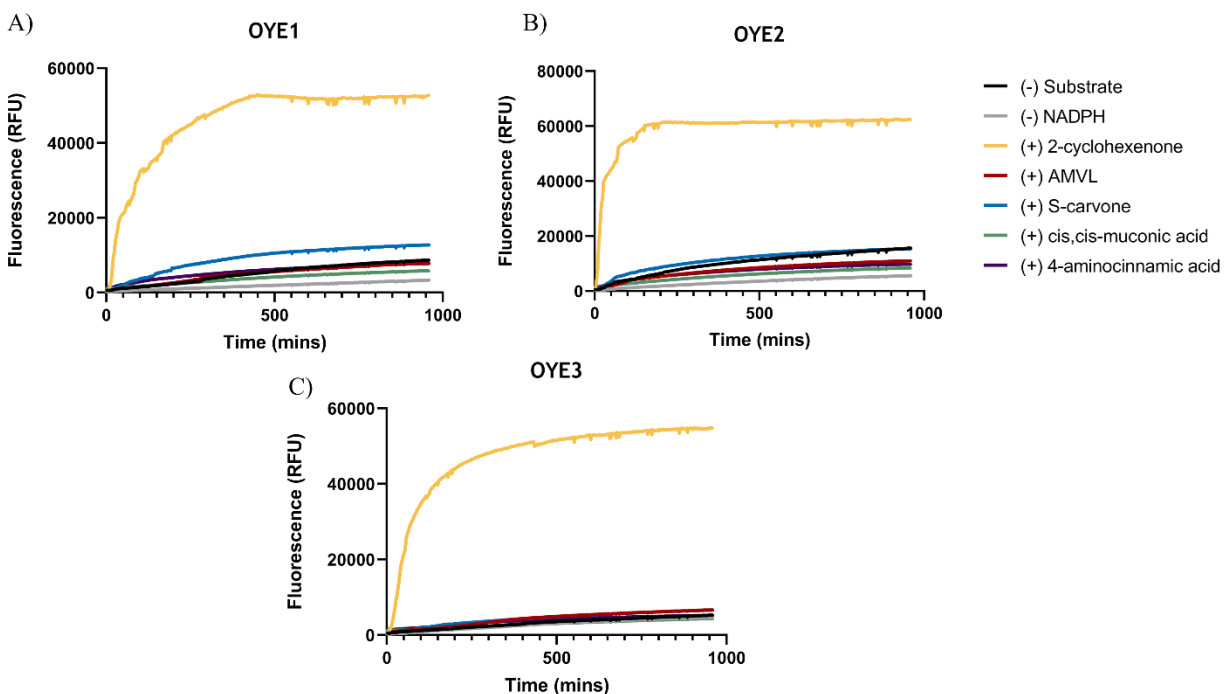
Figure 12. Results of Screening Assay with Class II OYEs. A) Activity of OYE1 against biopolymer precursors. Assay was performed at 37C for 16 hours with fluorescence measurements every 3 minutes at 445 nm. B) Activity of OYE2 against biopolymer precursors. Assay was performed at 37C for 16 hours with fluorescence measurements every 3 minutes at 445 nm. C) Activity of OYE3 against biopolymer precursors. Assay was performed at 37C for 16 hours with fluorescence measurements every 3 minutes at 445 nm.

Secondly, these results are unexpected as OYE2 does not show activity on AMVL. AMVL was generously generated by the Hoye lab (University of Minnesota) and its presence in solution was verified by direct injection mass spectrometry (Supplemental Figure A1). OYE2 has previously been reported to reduce AMVL to (−)-β-methyl-δ-valerolactone [105] and enzyme kinetics have been established for this reaction by measuring the oxidation of NADPH at 340 nm (K_M = 90±5 mM and k_{cat} = 0.04±0.02 s^{-1}). As the K_M for this reported reaction is substantially higher than the concentration of AMVL used in the screening (1 mM AMVL), it was thought that the concentration of AMVL simply wasn't high enough to have activity captured by the fluorescence-based activity assay. To investigate this, the activity of OYE2 on AMVL was measured through the oxidation of NADPH at 340 nm as was done originally in literature [105].

However, as shown in Appendix A.2 and Supplementary Figure A4, this activity could not be observed by traditional absorbance methods either.
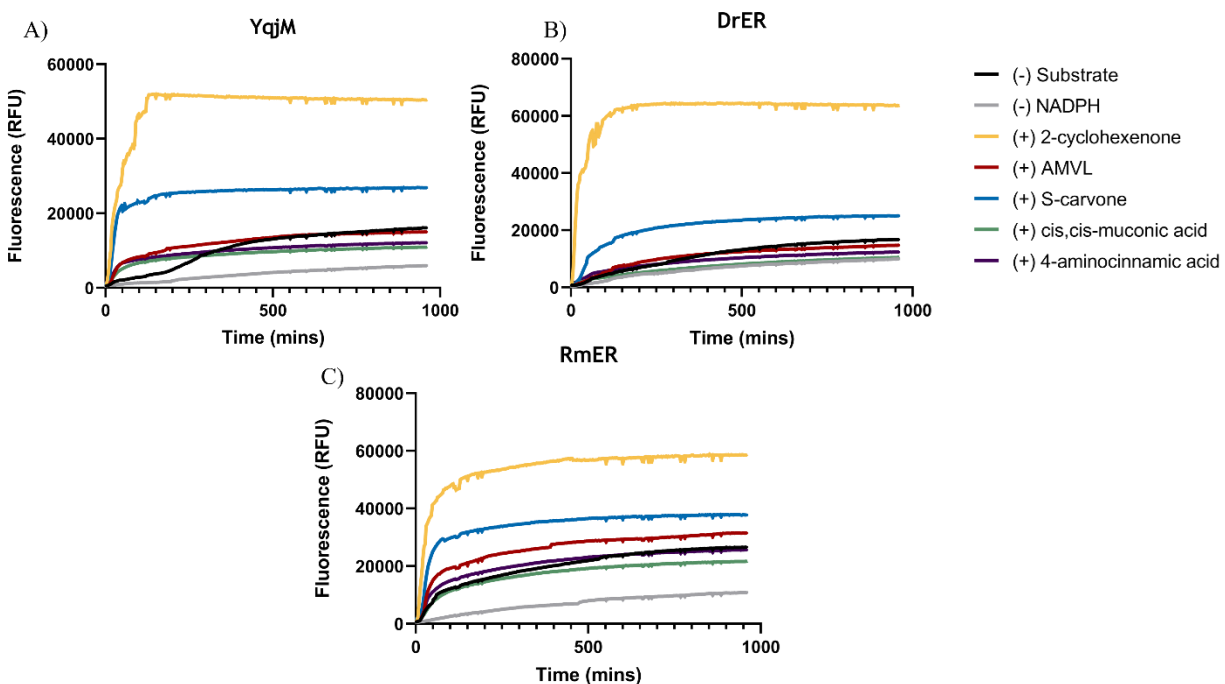
Figure 13. Results of Screening Assay with Class III OYEs. A) Activity of YqjM against biopolymer precursors. Assay was performed at 37C for 16 hours with fluorescence measurements every 3 minutes at 445 nm. B) Activity of DrER against biopolymer precursors. Assay was performed at 37C for 16 hours with fluorescence measurements every 3 minutes at 445 nm. C) Activity of RmER against biopolymer precursors. Assay was performed at 37C for 16 hours with fluorescence measurements every 3 minutes at 445 nm.

Finally, Figure 13 shows the results of the screening with the Class III OYEs. As with the Class I OYEs, all three Class III OYEs show activity on S-(+)-carvone, as expected [153] [159]. Comparing between the three enzymes, the reaction containing YqjM has the fastest rate of fluorescence generation when S-(+)-carvone is the given substrate with an increase of 187 RFU/min in the first 30 minutes of the reaction compared to DrER's 36 RFU/min and RmER's 156 RFU/min. However, at the end of the 16 hours, RmER's activity on S-(+)-carvone generates significantly higher fluorescence than YqjM or DrER ($p = 0.0150$ and $p = 0.0001$, respectively). Beyond S-(+)-carvone, the Class III OYEs follow a similar pattern to the first two classes and do not have any significant activity on the other biopolymer precursors. In contrast to the other two classes, however, the off-target fluorescence found in the (-) substrate controls is much higher and follows an initial trajectory akin to an OYE reducing a substrate in the RmER and DrER screens. With this in mind, a replicate screening was done with RmER and DrER to investigate if there was

some activity lost in the initial screen to this off-target fluorescence.

The results of this replicate screen can be found in Supplementary Figure A5. As shown, the results are similar to the initial screen. By the 16-hour criteria, only the fluorescence generated by the S-(+)-carvone can be considered a hit as it is statistically significantly different to the (-) substrate control for both RmER and DrER (p = 0.0025 and p = 0.0002, respectively). The other biopolymer precursor reactions fail to be significant against their respective (-) substrate controls at 16 hours. However, the earlier phase of both reactions may reveal a different story. At 80 minutes, both RmER and DrER have statistically significantly higher fluorescence on 4-ACA compared to their (-) substrate controls (p = 0.0025, p = 0.0002). As stated above, 4-ACA is a precursor to 4-aminohydrocinnamic acid (4-AHCA) which can be polymerized into polyamide plastics [160]. In the original paper discussing the use of enoate reductases in the bioproduction of this polyamide, an iron-sulfur enoate reductase was used. This iron-sulfur enoate reductase (ca2ENR) shares functional similarity to the OYEs in this work however unlike OYEs, like other clostridial enoate reductases, ca2ENR is oxygen-sensitive and thus needs to be handled in an anaerobic or microanaerobic environment *in vitro* [161] [162] which may present difficulties in a large-scale, industrial context. For the reduction of 4-ACA to 4-AHCA, Minakawa et al. [160] investigated an OYE as well as ca2ENR: XenB. XenB belongs to the class I family of OYEs but was not able to reduce 4-ACA in their conditions. In contrast, Supplementary Figure A5 shows two OYEs that may be able to reduce 4-ACA in RmER and DrER. With this in mind, we sought to further investigate this potential reduction of 4-ACA by RmER and DrER by liquid chromatography-mass spectrometry (LC-MS).

3.7 - Investigation into 4-ACA Reduction by RmER and DrER via LC-MS

To test whether RmER and DrER indeed catalyze the reduction of 4-ACA, LC-MS was used. In their earlier work, Minakawa et al. [160] used HPLC to confirm the consumption of 4-ACA and the production of 4-AHCA by ca2ENR. Reactions containing 5 mM 4-ACA, 2 mM NADPH, and 5 µg of either RmER or DrER were incubated at 37 °C overnight before separation on the LC-MS.
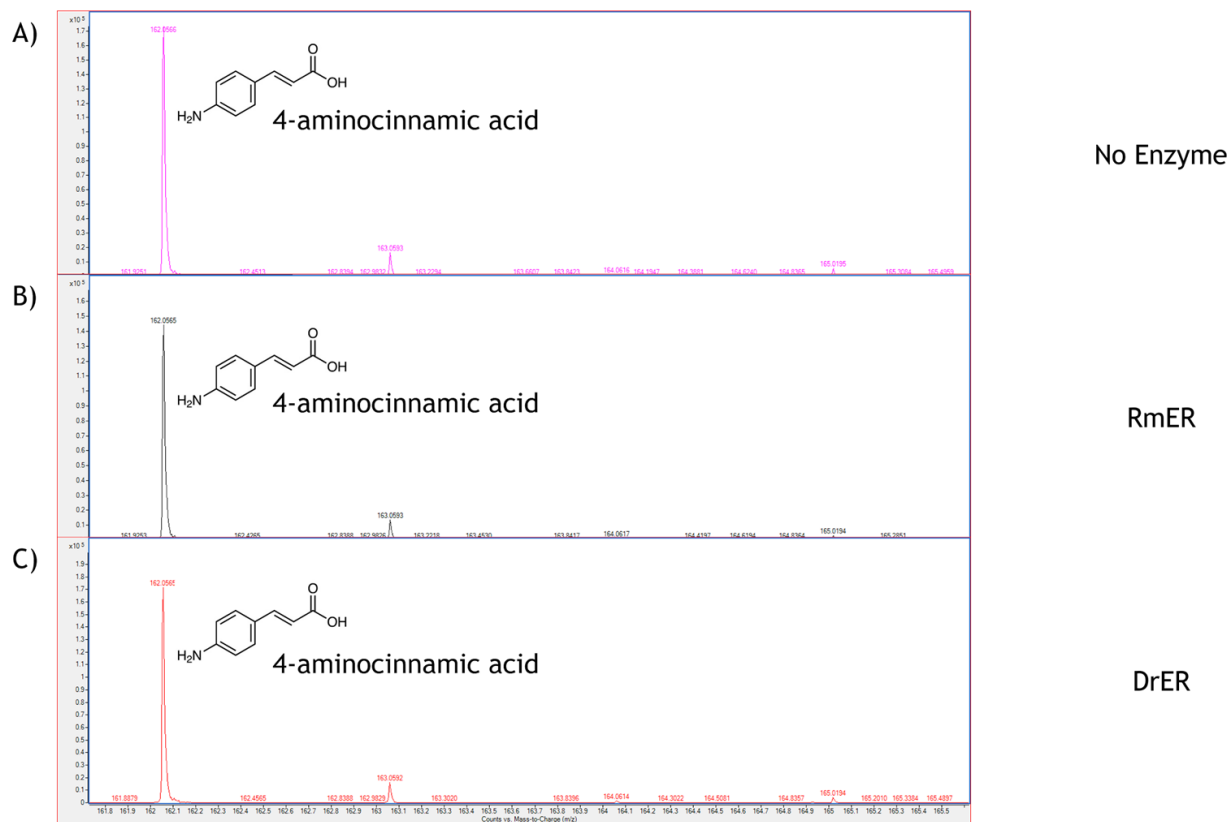
Figure 14. Disconfirmation of 4-ACA reduction by RmER or DrER via LC-MS. A) Mass spectra following separation of 5mM 4-ACA standard. Peak at 162 m/z corresponds well to 4-ACA ([M – H]⁻). Sample analyzed in negative mode. B) Mass spectra following overnight incubation of 5 mM 4-ACA with RmER. Sample separated and analyzed in negative mode. Peak at 162 m/z corresponds well to 4-ACA ([M – H]⁻). C) Mass spectra following overnight incubation of 5 mM 4-ACA with DrER. Sample separated and analyzed in negative mode. Peak at 162 m/z corresponds well to 4-ACA ([M – H]⁻).

As shown in Figure 14A, 4-ACA alone can be detected at a m/z of 162.0566 while running the MS in negative mode which corresponds well to the exact mass of 4-ACA (163.0633 Da) stripped of a proton. As the addition of two hydrogens is expected by the mechanism of both RmER and DrER, a successful reduction of 4-ACA is expected to garner a peak at 164.0717 m/z corresponding to deprotonated 4-AHCA. However, as shown in Figure 14B and Figure 14C, this peak is not seen in the overnight reaction of either RmER or DrER while the peak at 162.0566 corresponding to 4-ACA is present. This result does not support the potential activity found within the replicate screening of RmER and DrER (Supplementary Figure A5), reinforcing the need for optimization of the fluorescence-based activity assay to decrease the amount of off-target fluorescence generated as this false hit was likely the result of this off-target fluorescence.

3.8 - Investigation into Off-Target Fluorescence via FMN Quantification

While somewhat present in all OYE screenings, off-target fluorescence is most prominent in the Class III OYEs. This result suggests that there is some intrinsic quality to the Class III enzymes that render them more susceptible to this off-target fluorescence than the other classes. These increased off-target effects also are present when measuring NADPH oxidation via absorbance (data not shown) which suggests nonspecific NADPH oxidation is driving the off-target fluorescence. The question remains as to why this nonspecific oxidation is occurring. One explanation may have to do with the more accessible active site of Class III OYEs. Published crystal structure of YqjM shows that the active site is more accessible to substrate binding compared to other OYE classes [85]. Elucidated crystal structure of other class III OYEs such as RmER [163] and TOYE [164] agree with this increased accessibility, suggesting that this is a conserved characteristic amongst the class III OYEs. In solving the crystal structure of RmER, Opperman notes that there seems to be transient dissociation of FMN away from the active site, potentially linked to transient dimerization of the enzyme. Taken together, the more accessible active site combined with the dissociation of FMN from RmER (and potentially all class III OYEs) may be driving nonspecific NADPH oxidation at a faster rate than the other classes of OYEs. As discussed above, molecular oxygen is known to accept electrons from reduced $FMNH_2$, generating H_2O_2 and regenerating FMN. If there is an excess of non-bound FMN in solution with the class III OYEs, the accessible active site may be allowing reduced $FMNH_2$ to escape to react with molecular oxygen and the non-bound FMN may be "slotting" into the active site to be reduced by NADPH. With this mechanism, the class III OYEs would generate more $NADP^+$ at a faster rate than the other classes with their less accessible active sites and would explain why off-target fluorescence is much more pronounced in class III than in the others.

To investigate if there is excess FMN driving this nonspecific NADPH oxidation FMN concentration was investigated for select OYE purifications. FMN content was assessed to determine the saturation level of each OYE. Since each OYE active site binds one FMN, ideally the concentration of FMN and OYE would be the same if the enzymes were fully saturated with the necessary molecule for the catalytic cycle. As discussed above, the off-target fluorescence seen in Class III OYEs may be due to an excess of FMN in the protein purifications. With this in mind, Table 3 shows the results of the quantification of FMN in select OYE purifications. Absorbance

at 450 nm caused by protein interference was subtracted from each condition by repeating the experiment with GapA (which does not contain FMN) as a control.

Table 3: Quantification of FMN Content in OYE Protein Purifications

Enzyme	Enzyme Concentration	FMN Content
nemA	9.44 μM	0.568 ± 0.098 μM
PETNR	6.89 μM	1.53 ± 0.094 μM
OYE1	13.33 μM	1.51 ± 0.089 μM
OYE3	10.81 μM	2.18 ± 0.035 μM
RmER	5.28 μM	2.39 ± 0.074 μM
YqjM	6.70 μM	5.45 ± 0.126 μM

As shown in Table 3, the content of FMN is not equimolar in any OYE protein purification, indicating that none of the protein purifications are fully saturated with the FMN responsible for the catalytic cycle. This result demonstrates that the OYEs utilized in this project are not likely at their highest activity. If correct, some purifications have almost 20x less FMN (nemA) present for utilization by the enzyme. This lack of saturation may explain the lack of activity in some OYEs through the screening. Moreover, there does not appear to be an excess of FMN in any of the selected purifications, including the class III OYEs. This indicates that it is not an excess of FMN driving the nonspecific oxidation of NADPH. However, RmER and YqjM are more saturated than the other OYEs shown in Table 3, with RmER having 45% saturation and YqjM having 81% saturation. This increased amount of FMN may still be driving the off-target NADPH oxidation as discussed above.

3.9 - Michaelis Menten Kinetics of OPR1 via NADPH Absorbance

To add an additional facet of usefulness to the fluorescence-based enzyme cascade, we assessed if it could be used for enzyme kinetic characterization. OPR1 activity on S-(+)-carvone was chosen as the model reaction for this investigation due to its low off-target fluorescence. As the OYE that generated the highest fluorescence when paired with S-(+)-carvone while generating the least amount of off-target fluorescence in its negative controls, OPR1 was chosen for further characterization. While it is known that OPR1 will convert S-(+)-carvone to dihydrocarvone [153],

enzyme kinetics for this reaction have not been elucidated. To supplement knowledge on OPR1's activity on S-(+)-carvone, enzyme kinetics were established for this reaction using the traditional NADPH absorbance method.
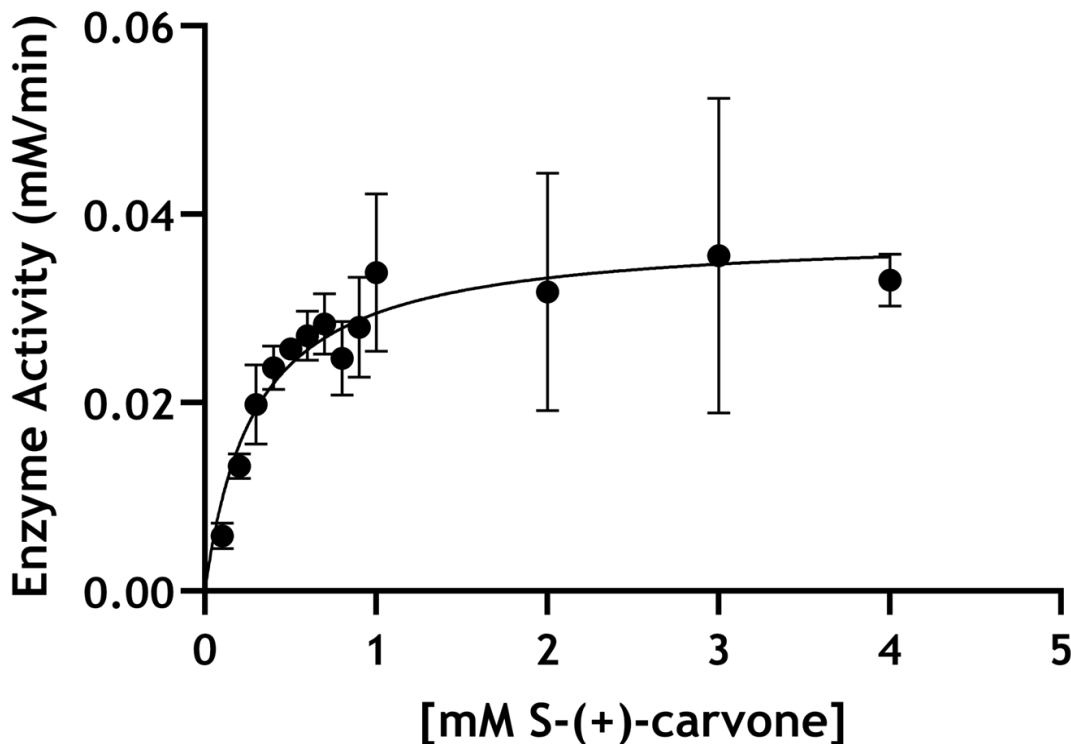
Figure 15. Michaelis-Menten Kinetics of OPR1 Against S-(+)-carvone via NADPH Oxidation. Investigation of Michaelis-Menten kinetics of OPR1 Against S-(+)-carvone via absorbance. Reaction measured at 340 nm every minute for 60 minutes.

Figure 15 shows thirteen concentrations of S-(+)-carvone that were investigated and we observed the above Michaelis-Menten curve for OPR1. The K_M for S-(+)-carvone was identified to be 0.29 mM and the turnover number (kcat) was found to be 10.8 s^{-1}. These values are in line with other OYEs and ene-reductases found in literature including the OYE ClER from *Clavispora lusitaniae* (K_M = 1.6 mM ± 0.1 , k_{cat} = 3.6 s^{-1} ± 0.1) [165], the OYEs PgOPR1 (K_M = 0.1181 mM, k_{cat} = 0.094 s^{-1}) PgOPR3 (K_M = 0.1495 mM, k_{cat} = 0.065 s^{-1}) from *Pelargonium graveolens* [166] and the F$_{420}$-dependent ene-reductases from *Mycobacterium smegmatis* MSMEG_2027 (K_M = 3.099 mM ± 0.9164, k_{cat} = 0.120 s^{-1} ± 0.0114) and MSMEG_2850 (K_M = 0.545 mM ± 0.1841, k_{cat} = 0.037 ± 0.0028 s^{-1}) [167]. One aspect that must be kept in mind is the low solubility of S-(+)-carvone in water that may impact the kinetic values presented here. While the data presented are

consistent with literature examples, other groups opted not to perform kinetic evaluations on OYEs that reduce either or both carvone enantiomers due to this poor solubility and its potential impact on the "true" activity of any given enzyme on carvone [125].

3.10 - Michaelis-Menten Kinetics of OPR1 via 4-Methylumbelliferone Fluorescence

Once the kinetics of OPR1 on S-(+)-carvone were established via the traditional NADPH absorbance method, I sought to examine whether similar kinetics could be established for the same reduction of S-(+)-carvone using the increase of 4-methylumbelliferone fluorescence through our fluorescence-based activity assay as an analogue to dihydrocarvone formation. This was investigated to assess if the fluorescence-based activity assay could be used to establish kinetics for redox enzymes going forward, replacing the traditional method, and adding an additional facet of usefulness to the fluorescence-based activity assay. To do this, first it was needed to establish the concentration of OPR1 at which the generation of 4-methylumbelliferone was rate-limited by OPR1's activity and not any of the supporting enzymes in the assay's cascade. This is necessary to establish whether or not the kinetics established through the ensuing fluorescence was OPR1's kinetics alone and not obfuscated by the activity of any of the supporting enzymes. To find the amount of OPR1 necessary to make it the rate-limiting step in the fluorescence-based activity assay, the rate of fluorescence generation must be plotted against OPR1 concentration. The range at which OPR1 is the rate-limiting enzyme will present as a linear segment of the aforementioned curve. Past this linear range, the rate of reaction is no longer dependent on OPR1 and will present as a plateau as the rate of fluorescence generation no longer increases linearly with the concentration of OPR1 in the assay. With this in mind, Figure 16A shows the linear range to be between 11 nM and 188 nM OPR and 94.31 nM (0.004 μg/μL) OPR1 was used to determine the Michaelis-Menten kinetics by fluorescence.
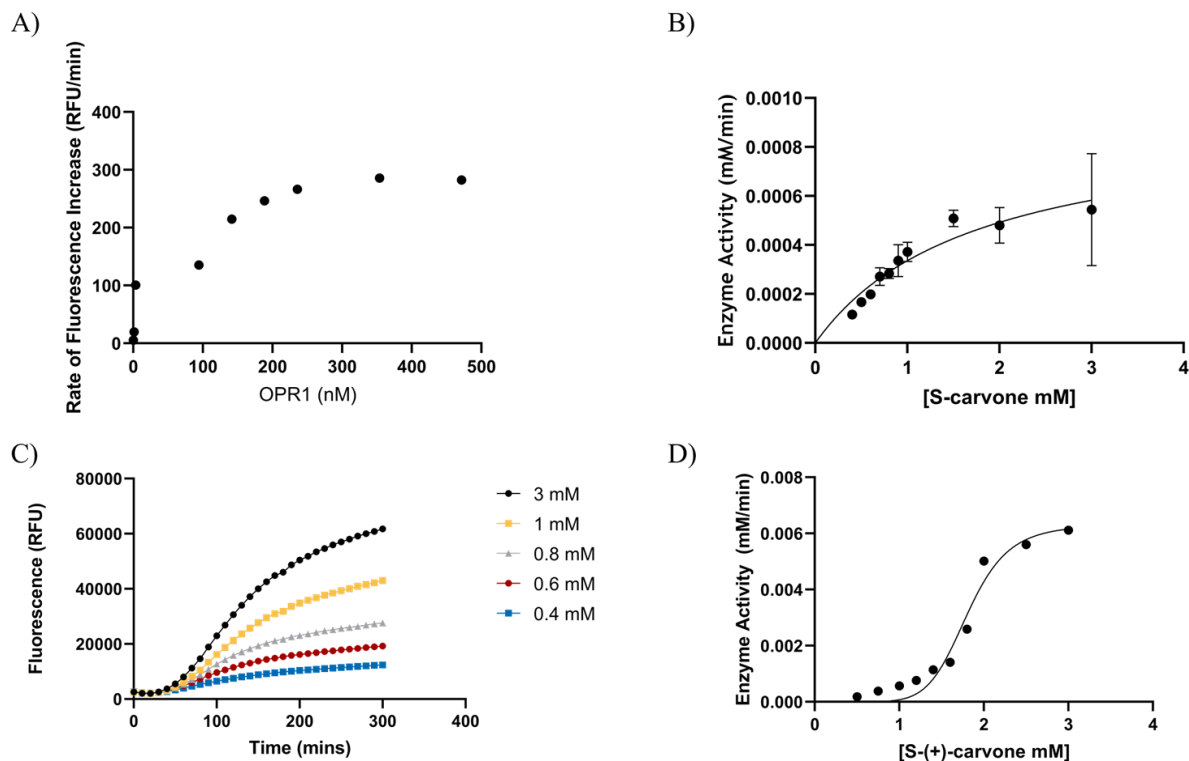
Figure 16. Investigation of Michaelis-Menten Kinetics of OPR1 vs S-(+)-carvone via Fluorescence-Based Activity Assay. A) Identification of linear range of OPR1 activity within the fluorescence-based activity assay which corresponds to OPR1 being the rate-limiting enzyme within the assay. Assay was performed for 3 hours, measuring fluorescence at 445 nm every minute. B) Michaelis-Menten kinetics of OPR1 (0.004 mg/mL) vs S-(+)-carvone via fluorescence. C) Fluorescence generation by OPR1 reducing different concentrations of S-(+)-carvone. Assay was performed over 5 hours with measurements taken every 10 minutes. D) Michaelis-Menten kinetics of OPR1 (0.1 mg/mL) vs S-(+)-carvone via fluorescence when OPR1 is not the rate limiting enzyme within the fluorescence cascade.

Figure 16B shows the Michaelis-Menten curve generated by utilizing OPR1 in the fluorescence-based activity assay. The K_M determined from this assay was 1.74 mM which is within the same order of magnitude with the previous K_M of OPR1/S-carvone found via the traditional NADPH oxidation assay. This indicates that the saturation of OPR1 with S-(+)-carvone is not greatly affected by the conditions supported by the fluorescence-based activity assay. However, the rate of enzyme activity does appear to be affected by these new conditions as k_{cat} was calculated to be 0.16 s^{-1}, about 100-fold less catalytic turnover than what was found via the absorbance assay. In order to perform Michaelis-Menten kinetics, some measurement of product formation is required. For the previous absorbance-based kinetics, product formation was equated with the oxidation of NADPH to NADP$^+$. For the fluorescence-based kinetics, this product

45

formation is instead equated to the release of 4-methylumbelliferone which occurs at the end of the enzymatic cascade. While I identified the linear range of OPR1 to account for the activity of the supporting enzymes within the cascade, the release of 4-methylumbelliferone is still dependent on four other enzymes with their own catalytic efficiencies and this may be impacting the speed at which 4-methylumbelliferone is released. As shown in Figure 16C there is a significant lag time before fluorescence begins to be read through 4-methylumbelliferone release. As Michaelis-Menten kinetics are dependent on the initial velocity of the enzyme to be able to calculate the rate of product formation, this lag may be interfering with this initial velocity calculation and thus the curve generated in Figure 16B is not truly representative of OPR1's action against S-(+)-carvone and is instead being modulated by the rest of the enzymatic cascade. This lag is potentially due to the allosteric nature of PgK. Figure 16D shows the Michaelis-Menten curve generated when OPR1 is not the rate-limiting enzyme within the fluorescence-based activity assay. In Figure 16B, OPR1 concentration is much lower than the supporting enzymes (0.004 mg/mL OPR1 vs 0.02 mg/mL GapA, PGK, BglK, BglA-2 as in Chapter 2.13) while in Figure 16D, OPR1 concentration is higher than the supporting enzymes (0.1 mg/mL) which leads OPR1 to not be the rate-limiting enzyme. When OPR1 is not rate-limiting, the Michaelis-Menten curve generated from the fluorescence-based activity assay takes on an allosteric-like curve, as shown in 18D. Due to this, there may be a "hold-up" that is happening at PgK as 1,3-biphosphoglycerate is being generated. When in the presence of low S-(+)-carvone (and thus low amounts of 1,3-biphosphogylcerate is being generated), there is a low rate of fluorescence generation. However, a switch occurs at higher concentrations of substrate and the rate of fluorescence generation drastically increases. While no longer the rate-limiting enzyme in Figure 16B, PgK may still be impacting the rate of fluorescence generation by causing a "holdup" of 1,3-biphosphoglycerate that is only resolved at higher concentrations. In this way, the initial velocity measured in Figure 16C is not linear according to OPR1's activity. Due to these reasons, the fluorescence-based activity assay is not appropriate for enzyme characterization through Michaelis-Menten kinetics at this time.

Chapter 4 – Conclusions and Future Perspectives

In this work we demonstrate the successful verification and partial optimization of a novel enzyme-coupled fluorescence-based assay for the detection of redox enzyme activity. The assay was successfully verified as functional with commercial enzyme malate dehydrogenase and was verified as functional with in-house purified OYEs. The assay was characterized as having a sensitivity to enzymes in the nM concentration range and a Z' score of 0.82, indicating an assay with a low degree of variability. Range finding of cofactor concentrations and mutation of the supporting enzyme GapA was done to optimize the assay for use as a screening tool for assessing nine OYE candidates' activity on established biopolymer precursors. With the fluorescence-based activity assay functional and optimized, this screening was done as a first application of this novel assay. Using this assay, we successfully identified activity on S-(+)-carvone with PETNR, OPR1, nemA, OYE1, RmER, DrER, and YqjM. While all of these activities were known to literature, these hits demonstrate a successful use-case with the screening assay, identifying activity on a target molecule that was not a positive control. Additionally, while the screening initially revealed potentially positive hits with RmER and DrER seeming active on 4-ACA, LC-MS confirmed that these hits were false positives and highlighted the need for further optimization. To increase the versatility of the assay, we also investigated if OYE kinetics could be characterized using the assay. Baseline kinetics for OPR1 against S-(+)-carvone were established and the same conditions' kinetics derived from the use of the fluorescence-based activity assay were established. Upon comparison, the K_M values derived from each technique were within the same order of magnitude but the k_{cat} derived from the fluorescence-based approach was almost 100-fold decreased compared to the baseline k_{cat}. With this in mind, the fluorescence-based activity assay should not be used for enzyme characterization at this time.

Taken together, we have developed, characterized, and optimized a novel NADPH-oxidation dependent fluorescence-based activity assay for use with redox enzymes. OYEs were used in this work for screening applications but other industrially relevant redox enzymes could be used with the assay for screening. Ketoreductases are some of the most widely used biocatalysts in industry [168] and require a NAD(P)H cofactor for catalysis. Ketoreductase

KRED1 was demonstrated in a biocatalytic pathway towards ipatasertib, a potent kinase inhibitor currently in clinical trials for prostate and breast cancer [169]. Zheng et al. engineered ketoreductase CgKR1 towards the production of a wide variety of chiral alcohols which are valuable intermediates in pharmaceutical synthesis [170]. The use of our fluorescence-based activity could be valuable in further engineering of ketoreductases and other redox enzymes. Furthermore, any enzyme activity that could be coupled to redox activity could also be used within this assay. Ongoing work in the Kwan lab is focused on coupling decarboxylase activity to the fluorescence-based assay through the use of carbonic anhydrase. As decarboxylases produce CO_2, carbonic anhydrase would utilize that CO_2 and oxidize NAD(P)H, coupling it to the release of 4-methylumbelliferone. Showing activity by this expanding of the coupling enzymes used could further deepen the robustness of the fluorescence-based activity assay.

In terms of the OYE screening, the nine candidates herein described are only a portion of the existing OYEs. Further screening efforts could expand to include other OYEs, both characterized and putative. Further work could also be done to investigate if the fluorescence-based activity assay can be utilized in an anaerobic environment for the study of enoate reductases. As stated in Chapter 1, enoate reductases are already known to have activity on biopolymer precursors but due to their inherent oxygen sensitivity, engineering efforts remain difficult. Assuming the fluorescence-based activity assay can be used in an anaerobic or microaerobic environment, barriers towards the directed evolution of these enoate reductases could be diminished. Not limited to biopolymer precursors, enoate reductases have also been shown towards the biosynthesis of 3-phenylpropanol, a commonly used fragrance and flavouring agent that is majorly derived from petrochemical sources [171]. Biosynthesis of this compound would contribute to lessening dependence on petrochemical sources for fine chemicals.

The paradigm shift towards bioplastics is a vital and necessary step towards mitigating dependence on fossil fuels. Bioplastic production through enzymatic catalysis remains an attractive option to fuel this change. However, the hill to climb is great and engineering efforts on enzyme, organism, and system level scales is going to be necessary to surmount the cost-effectiveness and efficiency of current plastic manufacturing. With tools such as our novel fluorescence-based activity assay, engineering goals towards more efficient and robust redox

enzymes become more attainable and have the potential to make plastics more sustainable.

References

1. PlasticsEurope, E. P. R. O. (2019). Plastics—the facts 2019. An analysis of European plastics production, demand and waste data. *PlasticEurope https://www. plasticseurope. org/en/resources/publications/1804-plastics-facts-2019*.

2. Lebreton, L., & Andrady, A. (2019). Future scenarios of global plastic waste generation and disposal. *Palgrave Communications,* 5(1), 1-11.

3. Geyer, R., Jambeck, J. R., & Law, K. L. (2017). Production, use, and fate of all plastics ever made. *Science advances*, *3*(7), e1700782.

4. Soeder, D. J., & Soeder, D. J. (2021). Fossil fuels and climate change. *Fracking and the Environment: A scientific assessment of the environmental risks from hydraulic fracturing and fossil fuels*, 155-185.

5. Butt, N., Beyer, H. L., Bennett, J. R., Biggs, D., Maggini, R., Mills, M., ... & Possingham, H. P. (2013). Biodiversity risks from fossil fuel extraction. *Science*, *342*(6157), 425-426.

6. Ramirez, M. I., Arevalo, A. P., Sotomayor, S., & Bailon-Moscoso, N. (2017). Contamination by oil crude extraction–Refinement and their effects on human health. *Environmental Pollution*, *231*, 415-425.

7. Keranen, K. M., Weingarten, M., Abers, G. A., Bekins, B. A., & Ge, S. (2014). Sharp increase in central Oklahoma seismicity since 2008 induced by massive wastewater injection. *Science*, *345*(6195), 448-451.

8. Sachs, J., Kroll, C., Lafortune, G., Fuller, G., & Woelm, F. (2022). *Sustainable development report 2022*. Cambridge University Press.

9. Unger, S. R., Hottle, T. A., Hobbs, S. R., Thiel, C. L., Campion, N., Bilec, M. M., & Landis, A. E. (2017). Do single-use medical devices containing biopolymers reduce the environmental impacts of surgical procedures compared with their plastic equivalents?. *Journal of health services research & policy*, *22*(4), 218-225.

10. Anastas, P., & Eghbali, N. (2010). Green chemistry: principles and practice. *Chemical Society Reviews*, *39*(1), 301-312.

11. Anastas, P. T., & Warner, J. C. (1998). Principles of green chemistry. *Green chemistry: Theory and practice*, *29*.

12. Zimmerman, J. B., Anastas, P. T., Erythropel, H. C., & Leitner, W. (2020). Designing for a green chemistry future. *Science*, *367*(6476), 397-400.

13. Gillet, S., Aguedo, M., Petitjean, L., Morais, A. R. C., da Costa Lopes, A. M., Łukasik, R. M., & Anastas, P. T. (2017). Lignin transformations for high value applications: towards targeted modifications using green chemistry. *Green Chemistry*, *19*(18), 4200-4233.

14. Sun, X., Wang, X., Sun, F., Tian, M., Qu, L., Perry, P., ... & Liu, X. (2021). Textile waste fiber regeneration via a green chemistry approach: a molecular strategy for sustainable fashion. *Advanced Materials*, *33*(48), 2105174.

15. Yang, W., Wang, J., Jiao, L., Song, Y., Li, C., & Hu, C. (2022). Easily recoverable and reusable p-toluenesulfonic acid for faster hydrolysis of waste polyethylene terephthalate. *Green Chemistry*, *24*(3), 1362-1372.

16. Jessop, P. G. (2011). Searching for green solvents. *Green Chemistry*, *13*(6), 1391-1398.

17. Wen, C., Yin, A., & Dai, W. L. (2014). Recent advances in silver-based heterogeneous catalysts for green chemistry processes. *Applied Catalysis B: Environmental*, *160*, 730-741.

18. Gola, D., Tyagi, P. K., Arya, A., Chauhan, N., Agarwal, M., Singh, S. K., & Gola, S. (2021). The impact of microplastics on marine environment: A review. *Environmental Nanotechnology, Monitoring & Management*, *16*, 100552.

19. Bajt, O. (2021). From plastics to microplastics and organisms. *FEBS Open bio*, *11*(4), 954-966.

20. Vethaak, A. D., & Legler, J. (2021). Microplastics and human health. *Science*, *371*(6530), 672-674.

21. Yang, Y., Huang, J., Zhang, R., & Zhu, J. (2017). Designing bio-based plasticizers: Effect of alkyl chain length on plasticization properties of isosorbide diesters in PVC blends. *Materials & Design*, *126*, 29-36.

22. Guindani, C., Candiotto, G., Araújo, P. H., Ferreira, S. R., de Oliveira, D., Wurm, F. R., & Landfester, K. (2020). Controlling the biodegradation rates of poly (globalide-co-ε-caprolactone) copolymers by post polymerization modification. *Polymer Degradation and Stability*, *179*, 109287.

23. Woodruff, M. A., & Hutmacher, D. W. (2010). The return of a forgotten polymer—Polycaprolactone in the 21st century. *Progress in polymer science*, *35*(10), 1217-1256.

24. Cipolatti, E. P., Pinto, M. C. C., Henriques, R. O., da Silva Pinto, J. C. C., de Castro, A. M., Freire, D. M. G., & Manoel, E. A. (2019). Enzymes in green chemistry: the state of the art in chemical transformations. *Advances in enzyme technology*, 137-151.

25. Binod, P., Gnansounou, E., Sindhu, R., & Pandey, A. (2019). Enzymes for second generation biofuels: recent developments and future perspectives. *Bioresource Technology Reports*, *5*, 317-325.

26. Wu, S., Snajdrova, R., Moore, J. C., Baldenius, K., & Bornscheuer, U. T. (2021). Biocatalysis: enzymatic synthesis for industrial applications. *Angewandte Chemie International Edition*, *60*(1), 88-119.

27. Sulaiman, S., You, D. J., Kanaya, E., Koga, Y., & Kanaya, S. (2014). Crystal structure and thermodynamic and kinetic stability of metagenome-derived LC-cutinase. *Biochemistry*, *53*(11), 1858-1869.

28. Ribitsch, D., Acero, E. H., Greimel, K., Dellacher, A., Zitzenbacher, S., Marold, A., ... & Guebitz, G. M. (2012). A new esterase from Thermobifida halotolerans hydrolyses polyethylene terephthalate (PET) and polylactic acid (PLA). *Polymers*, *4*(1), 617-629.

29. Wei, R., Oeser, T., Then, J., Kühn, N., Barth, M., Schmidt, J., & Zimmermann, W. (2014). Functional characterization and structural modeling of synthetic polyester-degrading hydrolases from Thermomonospora curvata. *AMB express*, *4*, 1-10.

30. Shah, M., Rajhans, S., Pandya, H. A., & Mankad, A. U. (2021). Bioplastic for future: A review then and now. *World Journal of Advanced Research and Reviews*, *9*(2), 056-067.

31. Ceresana. "Bioplastics - Study: Market, Analysis, Trends - Ceresana". www.ceresana.com. Archived from the original on 4 November 2017. Retrieved 22 November 2022.

32. Djukić-Vuković, A., Mladenović, D., Ivanović, J., Pejin, J., & Mojović, L. (2019). Towards sustainability of lactic acid and poly-lactic acid polymers production. *Renewable and Sustainable Energy Reviews*, *108*, 238-252.

33. González, M. I., Alvarez, S., Riera, F., & Alvarez, R. (2007). Economic evaluation of an integrated process for lactic acid production from ultrafiltered whey. *Journal of food engineering*, *80*(2), 553-561.

34. Ge, X. Y., Qian, H., & Zhang, W. G. (2009). Improvement of l-lactic acid production from Jerusalem artichoke tubers by mixed culture of Aspergillus niger and Lactobacillus sp. *Bioresource Technology*, *100*(5), 1872-1874.

35. Zhu, Y., Lee, Y. Y., & Elander, R. T. (2007). Conversion of aqueous ammonia-treated corn stover to lactic acid by simultaneous saccharification and cofermentation. *Applied biochemistry and biotechnology*, *137*, 721-738.

36. Wellenreuther, C., Wolf, A., & Zander, N. (2021). *Cost structure of bio-based plastics: A Monte-Carlo-analysis for PLA* (No. 197). HWWI Research Paper.

37. Mike. (2023). *Polystyrene (PS) price index*. businessanalytiq. https://businessanalytiq.com/procurementanalytics/index/polystyrene-ps-price-index/

38. Zhang, Z., Li, Y., Zhang, J., Peng, N., Liang, Y., & Zhao, S. (2020). High-titer lactic acid production by Pediococcus acidilactici PA204 from corn stover through fed-batch simultaneous saccharification and fermentation. *Microorganisms*, *8*(10), 1491.

39. Singhvi, M., Gurjar, G., Gupta, V., & Gokhale, D. (2015). Biocatalyst development for lactic acid production at acidic pH using inter-generic protoplast fusion. *RSC advances*, *5*(3), 2024-2031.

40. Lassalle, V. L., & Ferreira, M. L. (2008). Lipase-catalyzed synthesis of polylactic acid: an overview of the experimental aspects. *Journal of Chemical Technology & Biotechnology: International Research in Process, Environmental & Clean Technology*, *83*(11), 1493-1502.

41. Yang, T. H., Kim, T. W., Kang, H. O., Lee, S. H., Lee, E. J., Lim, S. C., ... & Lee, S. Y. (2010). Biosynthesis of polylactic acid and its copolymers using evolved propionate CoA transferase and PHA synthase. *Biotechnology and bioengineering*, *105*(1), 150-160.

42. Annamalai, N., & Sivakumar, N. (2016). Production of polyhydroxybutyrate from wheat bran hydrolysate using Ralstonia eutropha through microbial fermentation. *Journal of Biotechnology*, *237*, 13-17.

43. Al-Battashi, H., Annamalai, N., Al-Kindi, S., Nair, A. S., Al-Bahry, S., Verma, J. P., & Sivakumar, N. (2019). Production of bioplastic (poly-3-hydroxybutyrate) using waste paper as a feedstock: Optimization of enzymatic hydrolysis and fermentation employing Burkholderia sacchari. *Journal of cleaner production*, *214*, 236-247.

44. Dey, S., & Tribedi, P. (2018). Microbial functional diversity plays an important role in the degradation of polyhydroxybutyrate (PHB) in soil. *3 Biotech*, *8*(3), 171.

45. Sobczak, L., Lang, R. W., & Haider, A. (2012). Polypropylene composites with natural fibers and wood–General mechanical property profiles. *Composites Science and Technology*, *72*(5), 550-557.

46. Bhola, S., Arora, K., Kulshrestha, S., Mehariya, S., Bhatia, R. K., Kaur, P., & Kumar, P. (2021). Established and emerging producers of PHA: Redefining the possibility. *Applied Biochemistry and Biotechnology*, *193*, 3812-3854.

47. Hori, C., Oishi, K., Matsumoto, K. I., Taguchi, S., & Ooi, T. (2018). Site-directed saturation mutagenesis of polyhydroxylalkanoate synthase for efficient microbial production of poly [(R)-2-hydroxybutyrate]. *Journal of bioscience and bioengineering*, *125*(6), 632-636.

48. Normi, Y. M., Hiraishi, T., Taguchi, S., Abe, H., Sudesh, K., Najimudin, N., & Doi, Y. (2005). Characterization and Properties of G4X Mutants of Ralstonia eutropha PHA Synthase for Poly (3-hydroxybutyrate) Biosynthesis in Escherichia coli. *Macromolecular bioscience*, *5*(3), 197-206.
49. Taguchi, S., & Doi, Y. (2004). Evolution of polyhydroxyalkanoate (PHA) production system by "enzyme evolution": successful case studies of directed evolution. *Macromolecular bioscience*, *4*(3), 145-156.
50. Polen, T., Spelberg, M., & Bott, M. (2013). Toward biotechnological production of adipic acid and precursors from biorenewables. *Journal of Biotechnology*, *167*(2), 75-84.
51. Yu, J. L., Xia, X. X., Zhong, J. J., & Qian, Z. G. (2014). Direct biosynthesis of adipic acid from a synthetic pathway in recombinant Escherichia coli. *Biotechnology and bioengineering*, *111*(12), 2580-2586.
52. Niu, W., Willett, H., Mueller, J., He, X., Kramer, L., Ma, B., & Guo, J. (2020). Direct biosynthesis of adipic acid from lignin-derived aromatics using engineered Pseudomonas putida KT2440. *Metabolic Engineering*, *59*, 151-161.
53. Saez-Jimenez, V., Scrima, S., Lambrughi, M., Papaleo, E., Mapelli, V., Engqvist, M. K., & Olsson, L. (2022). Directed Evolution of (R)-2-Hydroxyglutarate Dehydrogenase Improves 2-Oxoadipate Reduction by 2 Orders of Magnitude. *ACS Synthetic Biology*, *11*(8), 2779-2790.
54. Joo, J. C., Khusnutdinova, A. N., Flick, R., Kim, T., Bornscheuer, U. T., Yakunin, A. F., & Mahadevan, R. (2017). Alkene hydrogenation activity of enoate reductases for an environmentally benign biosynthesis of adipic acid. *Chemical science*, *8*(2), 1406-1413.
55. Zhang, H., Li, Z., Pereira, B., & Stephanopoulos, G. (2015). Engineering E. coli–E. coli cocultures for production of muconic acid from glycerol. *Microbial cell factories*, *14*, 1-10.
56. Curran, K. A., Leavitt, J. M., Karim, A. S., & Alper, H. S. (2013). Metabolic engineering of muconic acid production in Saccharomyces cerevisiae. *Metabolic engineering*, *15*, 55-66.
57. Jung, H. M., Jung, M. Y., & Oh, M. K. (2015). Metabolic engineering of Klebsiella pneumoniae for the production of cis, cis-muconic acid. *Applied microbiology and biotechnology*, *99*, 5217-5225.
58. Toogood, H. S., & Scrutton, N. S. (2014). New developments in 'ene'-reductase catalysed biological hydrogenations. *Current opinion in chemical biology*, *19*, 107-115.
59. Toogood, H. S., & Scrutton, N. S. (2018). Discovery, characterization, engineering, and applications of ene-reductases for industrial biocatalysis. *ACS catalysis*, *8*(4), 3532-3549.
60. Stuermer, R., Hauer, B., Hall, M., & Faber, K. (2007). Asymmetric bioreduction of activated C= C bonds using enoate reductases from the old yellow enzyme family. *Current opinion in chemical biology*, *11*(2), 203-213.
61. Warburg, O., & Christian, W. (1933). The yellow oxidizing enzyme. *Biochem. Ztschr.*, *258*, 496-498.
62. Theorell, H. (1935). Das gelbe Oxydationsferment. *Biochem. z*, *278*, 263-290.
63. Breithaupt, C., Strassner, J., Breitinger, U., Huber, R., Macheroux, P., Schaller, A., & Clausen, T. (2001). X-ray structure of 12-oxophytodienoate reductase 1 provides structural insight into substrate binding and specificity within the family of OYE. *Structure*, *9*(5), 419-429.

64. Robescu, M. S., Niero, M., Hall, M., Cendron, L., & Bergantino, E. (2020). Two new ene-reductases from photosynthetic extremophiles enlarge the panel of old yellow enzymes: Ct OYE and Gs OYE. *Applied microbiology and biotechnology*, *104*, 2051-2066.

65. Miura, K., Tomioka, Y., Suzuki, H., YONEZAWA, M., Hishinuma, T., & Mizugaki, M. (1997). Molecular cloning of the nemA gene encoding N-ethylmaleimide reductase from Escherichia coli. *Biological and Pharmaceutical Bulletin*, *20*(1), 110-112.

66. Karplus, P. A., Fox, K. M., & Massey, V. (1995). Structure-function relations for old yellow enzyme. *The FASEB journal*, *9*(15), 1518-1526.

67. Kohli, R. M., & Massey, V. (1998). The oxidative half-reaction of Old Yellow Enzyme: the role of tyrosine 196. *Journal of biological chemistry*, *273*(49), 32763-32770.

68. Williams, R. E., & Bruce, N. C. (2002). 'New uses for an old enzyme'–the old yellow enzyme family of flavoenzymes. *Microbiology*, *148*(6), 1607-1614.

69. Amato, E. D., & Stewart, J. D. (2015). Applications of protein engineering to members of the old yellow enzyme family. *Biotechnology Advances*, *33*(5), 624-631.

70. Haarer, B. K., & Amberg, D. C. (2010). Retraction for Old Yellow Enzyme Protects the Actin Cytoskeleton from Oxidative Stress. *Molecular Biology of the Cell*, *21*(5), 842–842.

71. Fitzpatrick, T. B., Amrhein, N., & Macheroux, P. (2003). Characterization of YqjM, an Old Yellow Enzyme homolog from Bacillus subtilis involved in the oxidative stress response. *Journal of biological chemistry*, *278*(22), 19891-19897.

72. Odat, O., Matta, S., Khalil, H., Kampranis, S. C., Pfau, R., Tsichlis, P. N., & Makris, A. M. (2007). Old yellow enzymes, highly homologous FMN oxidoreductases with modulating roles in oxidative stress and programmed cell death in yeast. *Journal of Biological Chemistry*, *282*(49), 36010-36023.

73. Trotter, E. W., Collinson, E. J., Dawes, I. W., & Grant, C. M. (2006). Old yellow enzymes protect against acrolein toxicity in the yeast Saccharomyces cerevisiae. *Applied and environmental microbiology*, *72*(7), 4885-4892.

74. Binks, P. R., French, C. E., Nicklin, S., & Bruce, N. C. (1996). Degradation of pentaerythritol tetranitrate by Enterobacter cloacae PB2. *Applied and Environmental Microbiology*, *62*(4), 1214-1219.

75. Fryszkowska, A., Toogood, H., Sakuma, M., Gardiner, J. M., Stephens, G. M., & Scrutton, N. S. (2009). Asymmetric reduction of activated alkenes by pentaerythritol tetranitrate reductase: specificity and control of stereochemical outcome by reaction optimisation. *Advanced synthesis & catalysis*, *351*(17), 2976-2990.

76. French, C. E., Nicklin, S., & Bruce, N. C. (1996). Sequence and properties of pentaerythritol tetranitrate reductase from Enterobacter cloacae PB2. *Journal of bacteriology*, *178*(22), 6623-6627.

77. French, C. E., & Bruce, N. C. (1994). Purification and characterization of morphinone reductase from Pseudomonas putida M10. *Biochemical Journal*, *301*(1), 97-103.

78. French, C. E., & Bruce, N. C. (1995). Bacterial morphinone reductase is related to Old Yellow Enzyme. *Biochemical Journal*, *312*(3), 671-678.

79. Bruce, N. C., Wilmot, C. J., Jordan, K. N., Trebilcock, A. E., Gray Stephens, L. D., & Lowe, C. R. (1990). Microbial degradation of the morphine alkaloids: identification of morphinone as an intermediate in the metabolism of morphine by Pseudomonas putida M10. *Archives of microbiology*, *154*, 465-470.

80. Fujimoto, T., Tomitaka, Y., Abe, H., Tsuda, S., Futai, K., & Mizukubo, T. (2011). Expression profile of jasmonic acid-induced genes and the induced resistance against the root-knot nematode (Meloidogyne incognita) in tomato plants (Solanum lycopersicum) after foliar treatment with methyl jasmonate. *Journal of plant physiology*, *168*(10), 1084-1097.

81. Stintzi, A., & Browse, J. (2000). The Arabidopsis male-sterile mutant, opr3, lacks the 12-oxophytodienoic acid reductase required for jasmonate synthesis. *Proceedings of the National Academy of Sciences*, *97*(19), 10625-10630.

82. Strassner, J., Schaller, F., Frick, U. B., Howe, G. A., Weiler, E. W., Amrhein, N., ... & Schaller, A. (2002). Characterization and cDNA-microarray expression analysis of 12-oxophytodienoate reductases reveals differential roles for octadecanoid biosynthesis in the local versus the systemic wound response. *The Plant Journal*, *32*(4), 585-601.

83. Scholtissek, A., Tischler, D., Westphal, A. H., Van Berkel, W. J., & Paul, C. E. (2017). Old yellow enzyme-catalysed asymmetric hydrogenation: linking family roots with improved catalysis. *Catalysts*, *7*(5), 130.

84. Toogood, H. S., Gardiner, J. M., & Scrutton, N. S. (2010). Biocatalytic reductions and chemical versatility of the old yellow enzyme family of flavoprotein oxidoreductases. *ChemCatChem*, *2*(8), 892-914.

85. Kitzing, K., Fitzpatrick, T. B., Wilken, C., Sawa, J., Bourenkov, G. P., Macheroux, P., & Clausen, T. (2005). The 1.3 Å crystal structure of the flavoprotein YqjM reveals a novel class of old yellow enzymes. *Journal of Biological Chemistry*, *280*(30), 27904-27913.

86. Opperman, D. J. (2017). Structural investigation into the C-terminal extension of the ene-reductase from Ralstonia (Cupriavidus) metallidurans. *Proteins: Structure, Function, and Bioinformatics*, *85*(12), 2252-2257.

87. Waller, J., Toogood, H. S., Karuppiah, V., Rattray, N. J. W., Mansell, D. J., Leys, D., ... & Scrutton, N. S. (2017). Structural insights into the ene-reductase synthesis of profens. *Organic & Biomolecular Chemistry*, *15*(20), 4440-4448.

88. Nizam, S., Gazara, R. K., Verma, S., Singh, K., & Verma, P. K. (2014). Comparative structural modeling of six old yellow enzymes (OYEs) from the necrotrophic fungus Ascochyta rabiei: insight into novel OYE classes with differences in cofactor binding, organization of active site residues and stereopreferences. *PloS one*, *9*(4), e95989.

89. Zhang, B., Zhang, Y., Collins, C. C., Johnson, D. I., & Zheng, Y. (1999). A built-in arginine finger triggers the self-stimulatory GTPase-activating activity of rho family GTPases. *Journal of Biological Chemistry*, *274*(5), 2609-2612.

90. Komoriya, Y., Ariga, T., Iino, R., Imamura, H., Okuno, D., & Noji, H. (2012). Principal role of the arginine finger in rotary catalysis of F1-ATPase. *Journal of Biological Chemistry*, *287*(18), 15134-15142.

91. Winkler, C. K., Tasnádi, G., Clay, D., Hall, M., & Faber, K. (2012). Asymmetric bioreduction of activated alkenes to industrially relevant optically active compounds. *Journal of biotechnology*, *162*(4), 381-389.

92. Li, Z., Wang, Z., Meng, G., Lu, H., Huang, Z., & Chen, F. (2018). Identification of an Ene Reductase from Yeast Kluyveromyces Marxianus and Application in the Asymmetric Synthesis of (R)-Profen Esters. *Asian Journal of Organic Chemistry*, *7*(4), 763-769.

93. Pietruszka, J., & Schölzel, M. (2012). Ene reductase-catalysed synthesis of (R)-profen derivatives. *Advanced synthesis & catalysis*, *354*(4), 751-756.

94. Shi, Q., Jia, Y., Wang, H., Li, S., Li, H., Guo, J., ... & You, S. (2021). Identification of four ene reductases and their preliminary exploration in the asymmetric synthesis of (R)-dihydrocarvone and (R)-profen derivatives. *Enzyme and Microbial Technology*, *150*, 109880.

95. Stueckler, C., Winkler, C. K., Bonnekessel, M., & Faber, K. (2010). Asymmetric synthesis of (R)-3-hydroxy-2-methylpropanoate ('Roche ester') and derivatives via biocatalytic C☐ C-bond reduction. *Advanced Synthesis & Catalysis*, *352*(14-15), 2663-2666.

96. Evans, D. A., Sacks, C. E., Kleschick, W. A., & Taber, T. R. (1979). Polyether antibiotics synthesis. Total synthesis and absolute configuration of the ionophore A-23187. *Journal of the American Chemical Society*, *101*(22), 6789-6791.

97. Nicolaou, K. C., Chakraborty, T. K., Piscopio, A. D., Minowa, N., & Bertinato, P. (1993). Total synthesis of rapamycin. *Journal of the American Chemical Society*, *115*(10), 4419-4420.

98. Brenna, E., Fuganti, C., & Serra, S. (2003). Enantioselective perception of chiral odorants. *Tetrahedron: asymmetry*, *14*(1), 1-42.

99. Brenna, E., Gatti, F. G., Monti, D., Parmeggiani, F., Sacchetti, A., & Valoti, J. (2015). Substrate-engineering approach to the stereoselective chemo-multienzymatic cascade synthesis of Nicotiana tabacum lactone. *Journal of Molecular Catalysis B: Enzymatic*, *114*, 77-85.

100. Feng, B., Li, X., Jin, L., Wang, Y., Tang, Y., Hua, Y., ... & Ying, X. (2022). Engineering the Activity of Old Yellow Enzyme NemR-PS for Efficient Reduction of (E/Z)-Citral to (S)-Citronellol. *Catalysts*, *12*(6), 631.

101. Ravelli, D., Protti, S., Neri, P., Fagnoni, M., & Albini, A. (2011). Photochemical technologies assessed: the case of rose oxide. *Green chemistry*, *13*(7), 1876-1884.

102. Reiße, S., Haack, M., Garbe, D., Sommer, B., Steffler, F., Carsten, J., ... & Brück, T. (2016). In vitro bioconversion of pyruvate to n-butanol with minimized cofactor utilization. *Frontiers in Bioengineering and Biotechnology*, *4*, 74.

103. Brenna, E., Crotti, M., Gatti, F. G., Monti, D., Parmeggiani, F., & Pugliese, A. (2017). One-pot multi-enzymatic synthesis of the four stereoisomers of 4-methylheptan-3-ol. *Molecules*, *22*(10), 1591.

104. Mouterde, L. M., Allais, F., & Stewart, J. D. (2018). Enzymatic reduction of levoglucosenone by an alkene reductase (OYE 2.6): a sustainable metal-and dihydrogen-free access to the bio-based solvent Cyrene®. *Green Chemistry*, *20*(24), 5528-5532.

105. Zhang, C., Schneiderman, D. K., Cai, T., Tai, Y. S., Fox, K., & Zhang, K. (2016). Optically active β-methyl-δ-valerolactone: Biosynthesis and polymerization. *ACS Sustainable Chemistry & Engineering*, *4*(8), 4396-4402.

106. Xiao, Y., Cummins, D., Palmans, A. R., Koning, C. E., & Heise, A. (2008). Synthesis of biodegradable chiral polyesters by asymmetric enzymatic polymerization and their formulation into microspheres. *Soft Matter*, *4*(3), 593-599.

107. Cywar, R. M., Zhu, J. B., & Chen, E. Y. X. (2019). Selective or living organopolymerization of a six-five bicyclic lactone to produce fully recyclable polyesters. *Polymer Chemistry*, *10*(23), 3097-3106.

108. Steinman, N. Y., & Domb, A. J. (2019). Injectable pasty biodegradable polyesters derived from castor oil and hydroxyl-acid lactones. *Journal of Pharmacology and Experimental Therapeutics*, *370*(3), 736-741.

109.		Oberleitner, N., Peters, C., Rudroff, F., Bornscheuer, U. T., & Mihovilovic, M. D. (2014). In vitro characterization of an enzymatic redox cascade composed of an alcohol dehydrogenase, an enoate reductases and a Baeyer–Villiger monooxygenase. *Journal of Biotechnology*, *192*, 393-399.

110.		Lowe, J. R., Martello, M. T., Tolman, W. B., & Hillmyer, M. A. (2011). Functional biorenewable polyesters from carvone-derived lactones. *Polymer Chemistry*, *2*(3), 702-708.

111.		Oberleitner, N., Ressmann, A. K., Bica, K., Gärtner, P., Fraaije, M. W., Bornscheuer, U. T., ... & Mihovilovic, M. D. (2017). From waste to value–direct utilization of limonene from orange peel in a biocatalytic cascade reaction towards chiral carvolactone. *Green chemistry*, *19*(2), 367-371.

112.		Kraus, G. A. (2008). Synthetic methods for the preparation of 1, 3-propanediol. *CLEAN–Soil, Air, Water*, *36*(8), 648-651.

113.		Sun, J., Raza, M., Sun, X., & Yuan, Q. (2018). Biosynthesis of adipic acid via microaerobic hydrogenation of cis, cis-muconic acid by oxygen-sensitive enoate reductase. *Journal of biotechnology*, *280*, 49-54.

114.		Hubbard, P. A., Liang, X., Schulz, H., & Kim, J. J. P. (2003). The crystal structure and reaction mechanism of Escherichia coli 2, 4-dienoyl-CoA reductase. *Journal of Biological Chemistry*, *278*(39), 37553-37560.

115.		Kawasaki, Y., Aniruddha, N., Minakawa, H., Masuo, S., Kaneko, T., & Takaya, N. (2018). Novel polycondensed biopolyamide generated from biomass-derived 4-aminohydrocinnamic acid. *Applied microbiology and biotechnology*, *102*, 631-639.

116.		Suvannasara, P., Tateyama, S., Miyasato, A., Matsumura, K., Shimoda, T., Ito, T., ... & Kaneko, T. (2014). Biobased polyimides from 4-aminocinnamic acid photodimer. *Macromolecules*, *47*(5), 1586-1593.

117.		Tateyama, S., Masuo, S., Suvannasara, P., Oka, Y., Miyazato, A., Yasaki, K., ... & Kaneko, T. (2016). Ultrastrong, transparent polytruxillamides derived from microbial photodimers. *Macromolecules*, *49*(9), 3336-3342.

118.		Ronova, I. A., & Bruma, M. (2010). Influence of chemical structure on glass transition temperature of polyimides. *Structural Chemistry*, *21*, 1013-1020.

119.		Brannigan, J. A., & Wilkinson, A. J. (2002). Protein engineering 20 years on. *Nature Reviews Molecular Cell Biology*, *3*(12), 964-970.

120.		Woodley, J. M. (2013). Protein engineering of enzymes for process applications. *Current opinion in chemical biology*, *17*(2), 310-316.

121.		Kazlauskas, R. J., & Bornscheuer, U. T. (2009). Finding better protein engineering strategies. *Nature chemical biology*, *5*(8), 526-529.

122.		Liu, Q., Xun, G., & Feng, Y. (2019). The state-of-the-art strategies of protein engineering for enzyme stabilization. *Biotechnology advances*, *37*(4), 530-537.

123.		Walton, A. Z., Conerly, W. C., Pompeu, Y., Sullivan, B., & Stewart, J. D. (2011). Biocatalytic reductions of Baylis–Hillman adducts. *Acs Catalysis*, *1*(9), 989-993.

124.		Reddy, T. N., & Rao, V. J. (2018). Importance of Baylis-Hillman adducts in modern drug discovery. *Tetrahedron letters*, *59*(30), 2859-2875.

125.		Padhi, S. K., Bougioukou, D. J., & Stewart, J. D. (2009). Site-saturation mutagenesis of tryptophan 116 of Saccharomyces pastorianus old yellow enzyme uncovers stereocomplementary variants. *Journal of the American Chemical Society*, *131*(9), 3271-3280.

126.   Nett, N., Duewel, S., Richter, A. A., & Hoebenreich, S. (2017). Revealing additional stereocomplementary pairs of old yellow enzymes by rational transfer of engineered residues. *ChemBioChem*, *18*(7), 685-691.

127.   Bougioukou, D. J., Kille, S., Taglieber, A., & Reetz, M. T. (2009). Directed evolution of an enantioselective enoate-reductase: testing the utility of iterative saturation mutagenesis. *Advanced synthesis & catalysis*, *351*(18), 3287-3305.

128.   Cobb, R. E., Chao, R., & Zhao, H. (2013). Directed evolution: past, present, and future. *AIChE Journal*, *59*(5), 1432-1440.

129.   Wang, Y., Xue, P., Cao, M., Yu, T., Lane, S. T., & Zhao, H. (2021). Directed evolution: methodologies and applications. *Chemical reviews*, *121*(20), 12384-12444.

130.   Madhavan, A., Arun, K. B., Binod, P., Sirohi, R., Tarafdar, A., Reshmy, R., ... & Sindhu, R. (2021). Design of novel enzyme biocatalysts for industrial bioprocess: Harnessing the power of protein engineering, high throughput screening and synthetic biology. *Bioresource Technology*, *325*, 124617.

131.   Daugherty, A. B., Govindarajan, S., & Lutz, S. (2013). Improved biocatalysts from a synthetic circular permutation library of the flavin-dependent oxidoreductase old yellow enzyme. *Journal of the American Chemical Society*, *135*(38), 14425-14432.

132.   Yu, Y., & Lutz, S. (2011). Circular permutation: a different way to engineer enzyme structure and function. *Trends in biotechnology*, *29*(1), 18-25.

133.   Brigé, A., Van Den Hemel, D., Carpentier, W., De Smet, L., & Van Beeumen, J. J. (2006). Comparative characterization and expression analysis of the four Old Yellow Enzyme homologues from Shewanella oneidensis indicate differences in physiological function. *Biochemical Journal*, *394*(1), 335-344.

134.   Sheng, X., Yan, M., Xu, L., & Wei, M. (2016). Identification and characterization of a novel Old Yellow Enzyme from Bacillus subtilis str. 168. *Journal of Molecular Catalysis B: Enzymatic*, *130*, 18-24.

135.   Fang, X., Zheng, Y., Duan, Y., Liu, Y., & Zhong, W. (2018). Recent advances in design of fluorescence-based assays for high-throughput screening. *Analytical chemistry*, *91*(1), 482-504.

136.   Mei, Z., Zhang, K., Qu, G., Li, J. K., Liu, B., Ma, J. A., ... & Sun, Z. (2020). High-throughput fluorescence assay for ketone detection and its applications in enzyme mining and protein engineering. *ACS omega*, *5*(23), 13588-13594.

137.   Nevolova, S., Manaskova, E., Mazurenko, S., Damborsky, J., & Prokop, Z. (2019). Development of fluorescent assay for monitoring of dehalogenase activity. *Biotechnology Journal*, *14*(3), 1800144.

138.   Moisă, M. E., Amariei, D. A., Nagy, E. Z., Szarvas, N., Toșa, M. I., Paizs, C., & Bencze, L. C. (2020). Fluorescent enzyme-coupled activity assay for phenylalanine ammonia-lyases. *Scientific Reports*, *10*(1), 18418.

139.   Kumagai, K., Kojima, H., Okabe, T., & Nagano, T. (2014). Development of a highly sensitive, high-throughput assay for glycosyltransferases using enzyme-coupled fluorescence detection. *Analytical biochemistry*, *447*, 146-155.

140.   Imamura, R. M., Kumagai, K., Nakano, H., Okabe, T., Nagano, T., & Kojima, H. (2019). Inexpensive high-throughput screening of kinase inhibitors using one-step enzyme-coupled fluorescence assay for ADP detection. *SLAS DISCOVERY: Advancing Life Sciences R&D*, *24*(3), 284-294.

141. Fabbro, D., Cowan-Jacob, S. W., & Moebitz, H. (2015). Ten things you should know about protein kinases: IUPHAR R eview 14. *British journal of pharmacology*, *172*(11), 2675-2700.

142. Zhang, Y., Werling, U., & Edelmann, W. (2014). Seamless ligation cloning extract (SLiCE) cloning method. *DNA Cloning and Assembly Methods*, 235-244.

143. Faeder, E. J., & Siegel, L. M. (1973). A rapid micromethod for determination of FMN and FAD in mixtures. *Analytical biochemistry*, *53*(1), 332-336.

144. Pesic, M., Fernández-Fueyo, E., & Hollmann, F. (2017). Characterization of the old yellow enzyme homolog from Bacillus subtilis (YqjM). *ChemistrySelect*, *2*(13), 3866-3871.

145. Salis, A., Cappai, L., Carucci, C., Parsons, D. F., & Monduzzi, M. (2020). Specific buffer effects on the intermolecular interactions among protein molecules at physiological pH. *The Journal of Physical Chemistry Letters*, *11*(16), 6805-6811.

146. Böhmer, S., Marx, C., Gómez-Baraibar, Á., Nowaczyk, M. M., Tischler, D., Hemschemeier, A., & Happe, T. (2020). Evolutionary diverse Chlamydomonas reinhardtii Old Yellow Enzymes reveal distinctive catalytic properties and potential for whole-cell biotransformations. *Algal Research*, *50*, 101970.

147. Slivinskaya, E. A., Plekhanova, N. S., Altman, I. B., & Yampolskaya, T. A. (2022). Engineering of Escherichia coli Glyceraldehyde-3-Phosphate Dehydrogenase with Dual NAD+/NADP+ Cofactor Specificity for Improving Amino Acid Production. *Microorganisms*, *10*(5), 976.

148. Walters, W. P., & Namchuk, M. (2003). Designing screens: how to make your hits a hit. *Nature reviews Drug discovery*, *2*(4), 259-266.

149. ZHANG, J., & OLDENBURG, K. R. (2009). Z-factor. *ratio*, *11*, 247-252.

150. Peatey, C. L., Spicer, T. P., Hodder, P. S., Trenholme, K. R., & Gardiner, D. L. (2011). A high-throughput assay for the identification of drugs against late-stage Plasmodium falciparum gametocytes. *Molecular and biochemical parasitology*, *180*(2), 127-131.

151. Li, M., Chen, X., Ye, Q. Z., Vogt, A., & Yin, X. M. (2012). A high-throughput FRET-based assay for determination of Atg4 activity. *Autophagy*, *8*(3), 401-412.

152. Mueller, N. J., Stueckler, C., Hauer, B., Baudendistel, N., Housden, H., Bruce, N. C., & Faber, K. (2010). The substrate spectra of pentaerythritol tetranitrate reductase, morphinone reductase, N-ethylmaleimide reductase and estrogen-binding protein in the asymmetric bioreduction of activated alkenes. *Advanced Synthesis & Catalysis*, *352*(2-3), 387-394.

153. Iqbal, N., Stewart, J. D., Macheroux, P., Rudroff, F., & Mihovilovic, M. D. (2018). Novel concurrent redox cascades of (R)-and (S)-carvones enables access to carvo-lactones with distinct regio-and enantioselectivity. *Tetrahedron*, *74*(52), 7389-7394.

154. Stueckler, C., Hall, M., Ehammer, H., Pointner, E., Kroutil, W., Macheroux, P., & Faber, K. (2007). Stereocomplementary bioreduction of α, β-unsaturated dicarboxylic acids and dimethyl esters using enoate reductases: enzyme-and substrate-based stereocontrol. *Organic letters*, *9*(26), 5409-5411.

155. Hall, M., Stueckler, C., Ehammer, H., Pointner, E., Oberdorfer, G., Gruber, K., ... & Faber, K. (2008). Asymmetric bioreduction of C☐ C bonds using enoate reductases

OPR1, OPR3 and YqjM: enzyme-based stereocontrol. *Advanced synthesis & catalysis*, *350*(3), 411-418.

156.   Crotti, M., Parmeggiani, F., Ferrandi, E. E., Gatti, F. G., Sacchetti, A., Riva, S., ... & Monti, D. (2019). Stereoselectivity switch in the reduction of α-alkyl-β-arylenones by structure-guided designed variants of the ene reductase OYE1. *Frontiers in Bioengineering and Biotechnology*, *7*, 89.

157.   Powell III, R. W., Buteler, M. P., Lenka, S., Crotti, M., Santangelo, S., Burg, M. J., ... & Stewart, J. D. (2018). Investigating Saccharomyces cerevisiae alkene reductase OYE 3 by substrate profiling, X-ray crystallography and computational methods. *Catalysis Science & Technology*, *8*(19), 5003-5016.

158.   Brown, B. J., Hyun, J. W., Duvvuri, S., Karplus, P. A., & Massey, V. (2002). The role of glutamine 114 in old yellow enzyme. *Journal of Biological Chemistry*, *277*(3), 2138-2145.

159.   Litthauer, S., Gargiulo, S., Van Heerden, E., Hollmann, F., & Opperman, D. J. (2014). Heterologous expression and characterization of the ene-reductases from Deinococcus radiodurans and Ralstonia metallidurans. *Journal of Molecular Catalysis B: Enzymatic*, *99*, 89-95.

160.   Minakawa, H., Masuo, S., Kaneko, T., & Takaya, N. (2019). Fermentation and purification of microbial monomer 4-amminocinnamic acid to produce ultra-high performance bioplastics. *Process Biochemistry*, *77*, 100-105.

161.   Mordaka, P. M., Hall, S. J., Minton, N., & Stephens, G. (2018). Recombinant expression and characterisation of the oxygen-sensitive 2-enoate reductase from Clostridium sporogenes. *Microbiology*, *164*(2), 122.

162.   Rohdich, F., Wiese, A., Feicht, R., Simon, H., & Bacher, A. (2001). Enoate reductases of Clostridia: Cloning, sequencing, and expression. *Journal of Biological Chemistry*, *276*(8), 5779-5787.

163.   Opperman, D. J. (2017). Structural investigation into the C-terminal extension of the ene-reductase from Ralstonia (Cupriavidus) metallidurans. *Proteins: Structure, Function, and Bioinformatics*, *85*(12), 2252-2257.

164.   Adalbjörnsson, B. V., Toogood, H. S., Fryszkowska, A., Pudney, C. R., Jowitt, T. A., Leys, D., & Scrutton, N. S. (2010). Biocatalysis with thermostable enzymes: structure and properties of a thermophilic 'ene'-reductase related to old yellow enzyme. *ChemBioChem*, *11*(2), 197-207.

165.   Ni, Y., Yu, H. L., Lin, G. Q., & Xu, J. H. (2014). An ene reductase from Clavispora lusitaniae for asymmetric reduction of activated alkenes. *Enzyme and microbial technology*, *56*, 40-45.

166.   Iijima, M., Kenmoku, H., Takahashi, H., Lee, J. B., Toyota, M., Asakawa, Y., ... & Taura, F. (2016). Characterization of 12-oxophytodienoic acid reductases from rose-scented geranium (pelargonium graveolens). *Natural Product Communications*, *11*(12), 1934578X1601101201.

167.   Kang, S. W., Antoney, J., Frkic, R. L., Lupton, D. W., Speight, R., Scott, C., & Jackson, C. J. (2022). Asymmetric Ene-Reduction of α, β-Unsaturated Compounds by F420-Dependent Oxidoreductases A Enzymes from Mycobacterium smegmatis. *Biochemistry*.

168.   Prier, C. K., & Kosjek, B. (2019). Recent preparative applications of redox enzymes. *Current Opinion in Chemical Biology*, *49*, 105-112.

169.   Han, C., Savage, S., Al-Sayah, M., Yajima, H., Remarchuk, T., Reents, R., ... & Gosselin, F. (2017). Asymmetric synthesis of Akt kinase inhibitor Ipatasertib. *Organic letters*, *19*(18), 4806-4809.

170.   Zheng, G. W., Liu, Y. Y., Chen, Q., Huang, L., Yu, H. L., Lou, W. Y., ... & Xu, J. H. (2017). Preparation of structurally diverse chiral alcohols by engineering ketoreductase Cg KR1. *ACS Catalysis*, *7*(10), 7174-7181.

171.   Liu, Z., Zhang, X., Lei, D., Qiao, B., & Zhao, G. R. (2021). Metabolic engineering of Escherichia coli for de novo production of 3-phenylpropanol via retrobiosynthesis approach. *Microbial Cell Factories*, *20*(1), 1-15.

Appendices

Appendix A: Supplemental Text

A.1 - Optimization of NADPH Concentration for Fluorescence-Based Activity Assay

Due to the substantial fluorescence found within samples containing Class III OYEs but no substrate, optimization of NADPH concentrations was done to ablate off-target fluorescence. As this off-target fluorescence is due to NADPH oxidation not dependent on an OYE reducing a substrate, this off-target fluorescence represents a significant limitation to the fluorescence-based activity assay. In ideal conditions, 1 molecule of NADPH being oxidized would correspond to 1 molecule of a substrate being reduced which would correspond to 1 molecule of 4-methylumbelliferone being released and fluorescing. This off-target fluorescence then does not conform to these ideal conditions. In addition, this off-target fluorescence may also be masking low-activity hits by outcompeting the 4-methylumbelliferone release driven by the low rate of conversion by some substrate by one of the Class III enzymes. To alleviate these concerns, differing concentrations of NADPH were tested with RmER in the fluorescence-based activity assay to determine the optimal NADPH level to decrease off-target fluorescence but remain abundant enough for the assay to proceed as designed.

As shown in Supplementary Figure A3, NADPH levels from 0.25 to 4 mM were examined. From the previous baseline of 1 mM NADPH, increasing NADPH levels widened the difference between positive and negative controls. However, at higher levels of NADPH (3 mM and 4 mM), wide variability between the positive and (-) substrate controls made the difference between them not significant as in the 1 mM NADPH condition (p = 0.13 and 0.11, at the end of 5 hours respectively). Decreasing the amount of NADPH present below 1 mM NADPH did not dampen the off-target fluorescence as compared to the 2-cyclohexenone control. From this investigation it was determined that the reaction with 2 mM NADPH significantly dampened the off-target fluorescence as opposed to the 1 mM NADPH condition while also not having large amount of variability found in the higher concentrations of NADPH (p = 0.001 at the end of 5 hours). Therefore, 2 mM NADPH was used in subsequent assays.

A.2 - Investigation into OYE2 Activity on AMVL

Recreating the experimental conditions from Zhang et al. [105], activity was present on 2-cyclohexenone represented by the decrease in absorbance of NADPH at 340 nm as it is oxidized by OYE2, shown in Supplementary Figure A4. This was not the case with any concentration of AMVL as the oxidation of NADPH by molecular oxygen ((-) substrate control) had a higher decrease in absorbance at 340nm than any of the reactions containing AMVL. The oxidation of NADPH by molecular oxygen is a known quantity when characterizing OYEs using the traditional absorbance method. In the absence of a given substrate, the FMN harbored within OYEs are able to utilize molecular oxygen as an oxidant to produce the reduced $FMNH_2$ which is able to oxidize NADH or NADPH into their respective oxidated states [158]. This catalytic activity has to be taken into account both in the fluorescence-based activity assay and in the traditional absorbance assay. As the lack of activity observed on AMVL by OYE2 is not confined to the context of the fluorescence-based activity assay and is also present in the traditional absorbance assay, this lack of activity must stem from issues beyond the context of the fluorescence-based activity assay.

Such issues could stem from the purification of OYE2 as our current purification is not exact to what was done in Zhang et al. [105], for example DTT is present in their lysis buffer and glycerol is present in the final storage buffer. Another source of issues could stem from potential introduced contaminations in the AMVL solution prepared by the Hoye lab. With these potential issues in mind, further investigation into OYE2 is necessary to determine the cause of this unexpected result.

Appendix B: Supplemental Figures
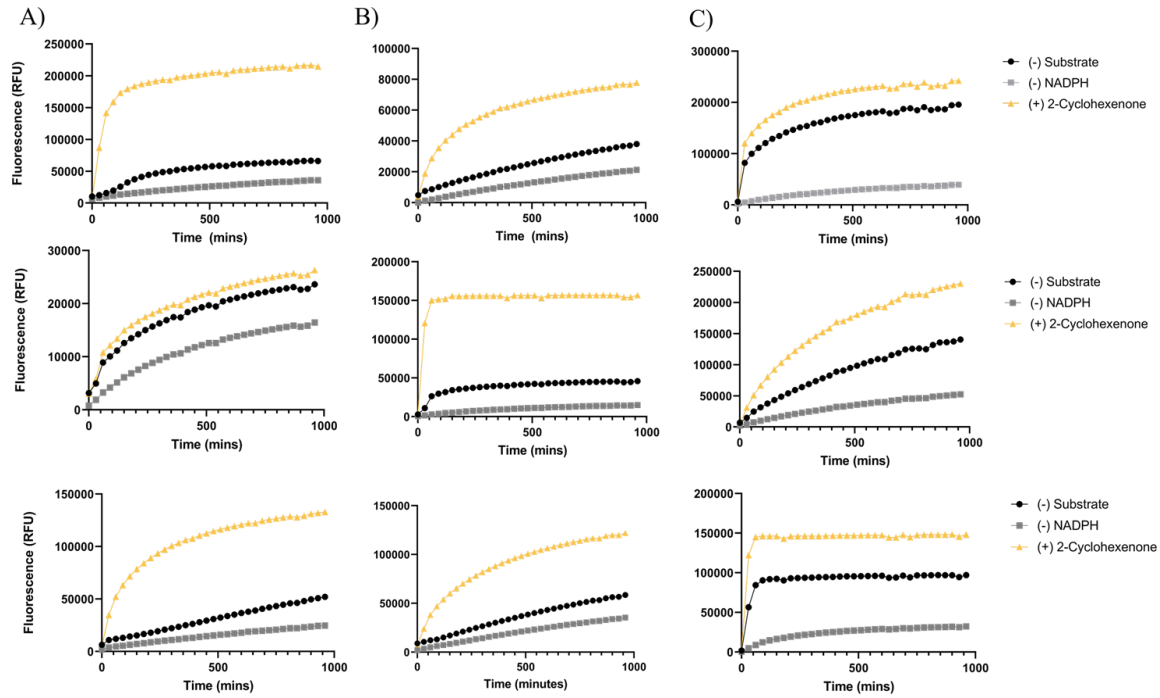
**Figure A1. Verification of OYE Function within Fluorescence-Based Activity Assay with Original Conditions**
A) Verification of Class I OYEs function. In descending order: nemA, OPR1, and PETNR. B)Verification of Class II OYEs function. In descending order: OYE1, OYE2, and OYE3. C)Verification of Class III function. In descending order: OYEs YqjM, DrER, and RmER.
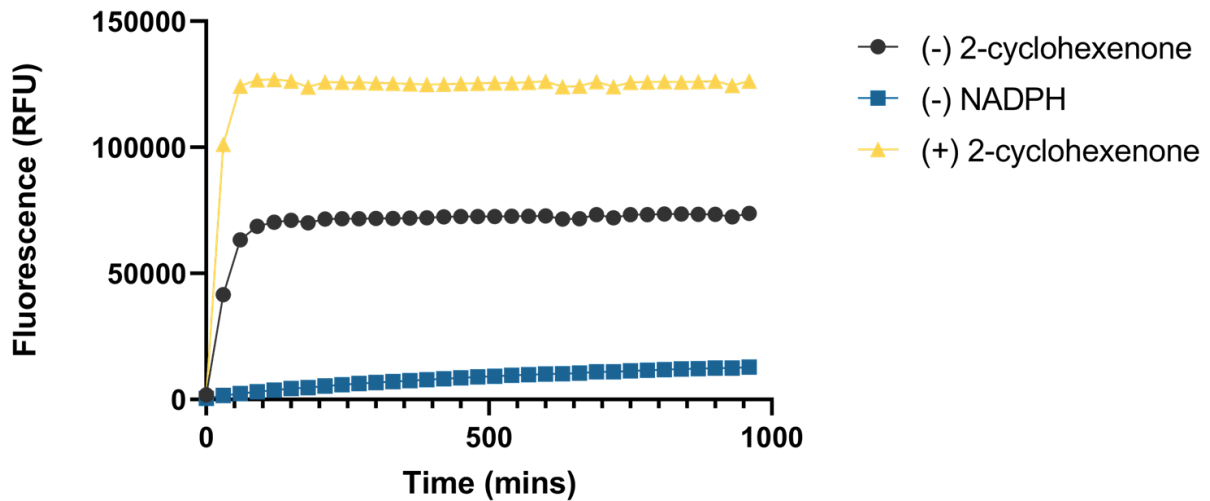

Figure A2. **Activity of Yqjm on 2-cyclohexenone After Purification Optimization.** Fluorescence was measured at 445 nm for 16 hours
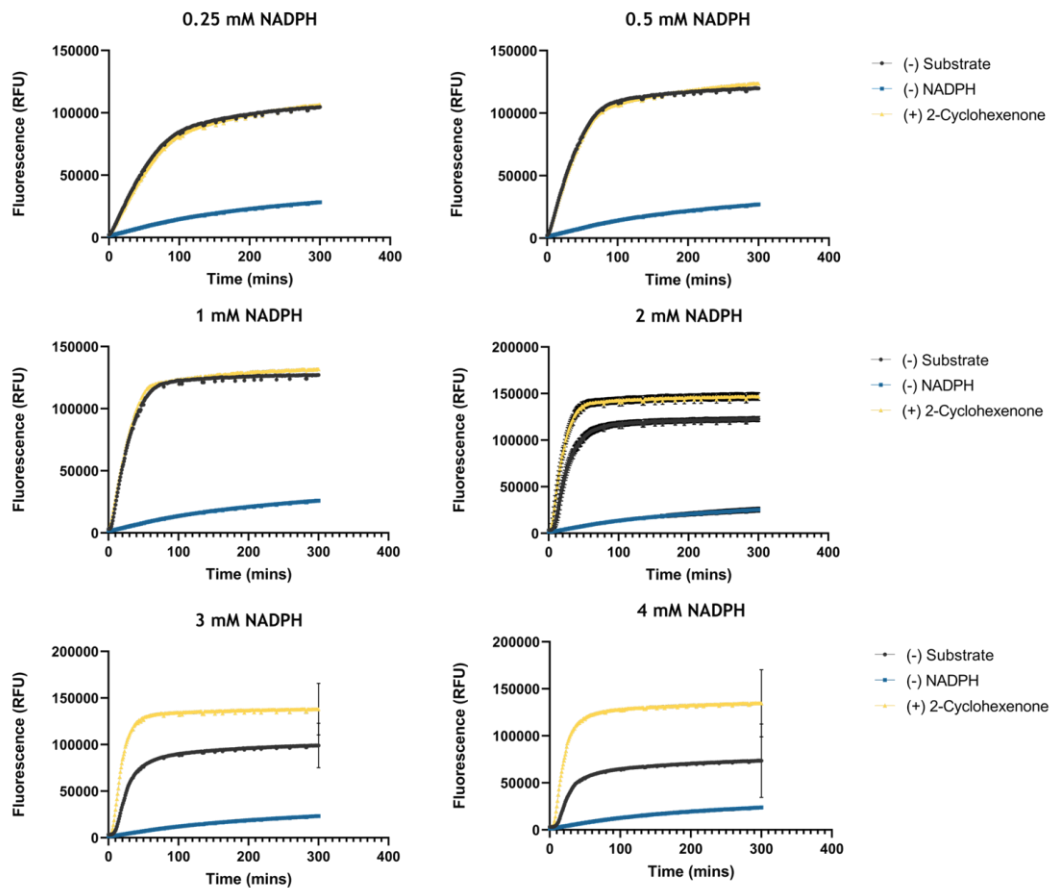
Figure A3. Optimization of NADPH Concentration to Ablate Off-Target Fluorescence. Differing NADPH concentrations were assessed to investigate off-target fluorescence. NADPH concentrations from 0.25 mM to 4 mM were incubated with 0.1 mg/mL RmER, 1 mM 2-cyclohexenone, and standard assay conditions. Fluorescence measured at 445 every minute for 5 hours.
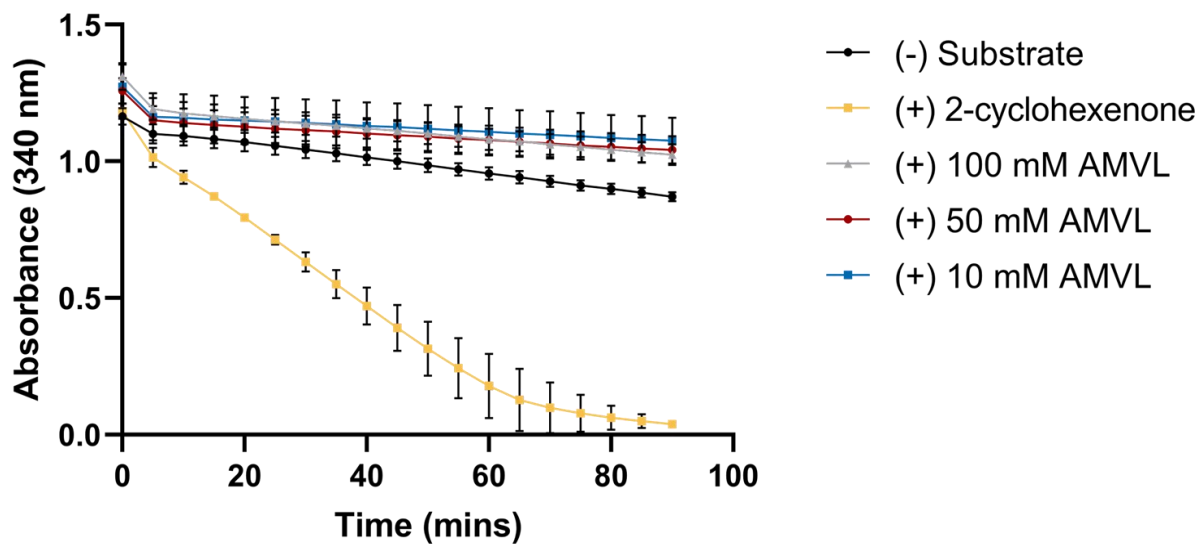
Figure A4. Investigation into Reduction of AMVL by OYE2 via Absorbance. OYE2 activity on AMVL was investigated via the decrease in absorbance of NADPH at 340 nm. Absorbance measured every 5 minutes at 340 nm.

A)

B)
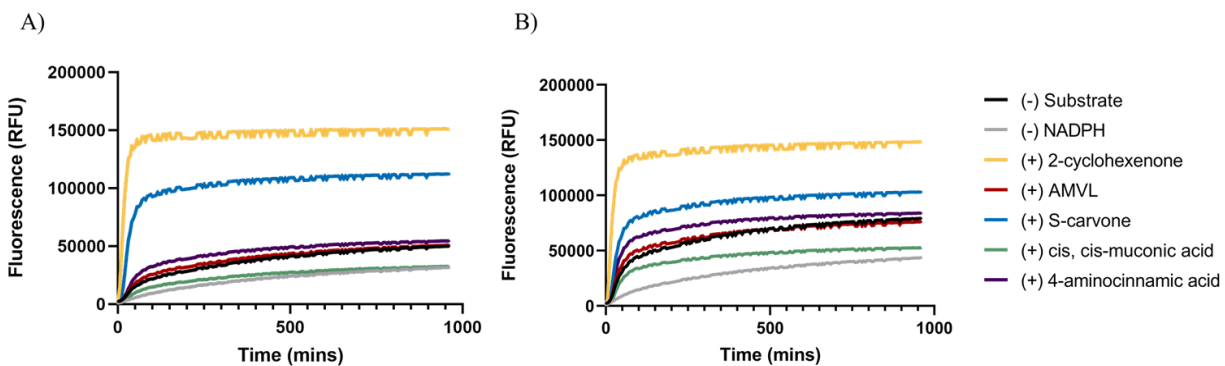
Figure A5. Replicate Screen of DrER and RmER Against Biopolymer Precursors. A) Activity of DrER against biopolymer precursors. Assay was performed at 37C for 16 hours with fluorescence measurements every 5 minutes at 445 nm. B) Activity of RmER against biopolymer precursors. Assay was performed at 37C for 16 hours with fluorescence measurements every 5 minutes at 445 nm.

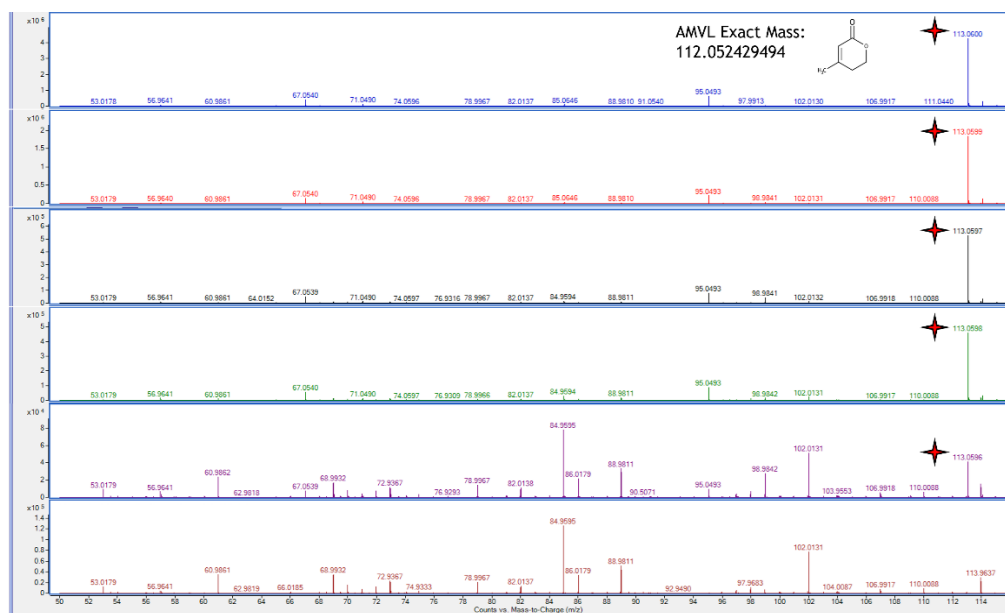**Figure A6. Direct Injection MS Spectra of Anhydromevalonolactone (AMVL).** AMVL purity was assessed via direct injection MS in positive mode. AMVL concentrations from 5 mM to 5µM were investigated.

Appendix C: Supplemental Tables

Table A1: Percent Sequence Identity of OYEs by ClustalW

	YqjM	DrER	RmER	OYE3	OYE1	OYE2	OPR	nemA	PETNR
YqjM	100	47.62	41.19	21.99	23.19	24.40	23.60	30.37	31.90
DrER	47.62	100	49.44	24.65	25.76	25.76	25.85	31.40	33.72
RmER	41.19	49.44	100	25.00	25.27	25.27	23.08	29.23	29.23
OYE3	21.99	24.65	25.00	100	80.25	81.50	38.65	39.61	38.50
OYE1	23.19	25.76	25.27	80.25	100	91.75	37.03	36.57	36.29
OYE2	24.40	25.76	25.27	81.50	91.75	100	37.30	36.84	36.84
OPR	23.60	25.85	23.08	38.65	37.03	37.30	100	41.62	42.46
nemA	30.37	31.40	29.23	39.61	36.57	36.84	41.62	100	87.67
PETNR	31.90	33.72	29.23	38.50	36.29	36.84	42.46	87.67	100